

INFORMATION TO USERS

This manuscript has been reproduced from the microfilm master. UMI films the text directly from the original or copy submitted. Thus, some thesis and dissertation copies are in typewriter face, while others may be from any type of computer printer.

The quality of this reproduction is dependent upon the quality of the copy submitted. Broken or indistinct print, colored or poor quality illustrations and photographs, print bleedthrough, substandard margins, and improper alignment can adversely affect reproduction.

In the unlikely event that the author did not send UMI a complete manuscript and there are missing pages, these will be noted. Also, if unauthorized copyright material had to be removed, a note will indicate the deletion.

Oversize materials (e.g., maps, drawings, charts) are reproduced by sectioning the original, beginning at the upper left-hand corner and continuing from left to right in equal sections with small overlaps.

Photographs included in the original manuscript have been reproduced xerographically in this copy. Higher quality 6" x 9" black and white photographic prints are available for any photographs or illustrations appearing in this copy for an additional charge. Contact UMI directly to order.

ProQuest Information and Learning
300 North Zeeb Road, Ann Arbor, MI 48106-1346 USA
800-521-0600

UMI[®]

RICE UNIVERSITY

Near Surface Seismic Imaging at a Porphyry Copper Mine

By

Diana Dana

**A THESIS SUBMITTED
IN PARTIAL FULFILLMENT OF THE
REQUIREMENTS FOR THE DEGREE**

Master of Arts

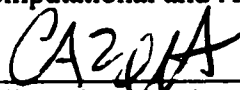
APPROVED, THESIS COMMITTEE:



**Alan Levander, Chairman, Carey Croneis
Professor of Earth Science**



**William Symes, Noah Harding Professor of
Computational and Applied Mathematics**



**Colin Zelt, Associate Professor of Earth
Science**



**Virginia B. Sisson, Clinical Assistant
Professor of Earth Science**

Houston, Texas

May, 2001

UMI Number: 1405656



UMI Microform 1405656

Copyright 2001 by Bell & Howell Information and Learning Company.

**All rights reserved. This microform edition is protected against
unauthorized copying under Title 17, United States Code.**

**Bell & Howell Information and Learning Company
300 North Zeeb Road
P.O. Box 1346
Ann Arbor, MI 48106-1346**

ABSTRACT

Near Surface Seismic Imaging at a Porphyry Copper Mine

By

Diana Dana

In June 1996, a 2-D high-resolution seismic survey was conducted at an open pit porphyry copper mine in southwest New Mexico. The local geology consists of a Miocene conglomerate, overlying Precambrian to Eocene basement rock containing unaltered igneous rock and mineralogically altered rock that hosts the sulfide deposits. The survey employed reflection and refraction techniques to image the top of the ore body. A variety of filtering techniques was used to suppress strong coherent source generated noise, and high amplitude ambient noise from mine operations. The resulting seismic sections compare well with borehole data and photographs of the mine walls; showing lithology and structural features within the initial 300 m of the subsurface. Imaging differences in lithology, contrasts due to sulfide deposition, and structures has potential importance for mine operations for efficiency of extraction and for safety. Locating structural features, such as those controlling groundwater flow, also has environmental applications.

ACKNOWLEDGEMENTS

I would like to thank a number of people who were associated with this project and those that provided support during its completion. First, thanks go to my advisors, Alan Levander and Colin Zelt, for entrusting this project to me. Thanks also go to the rest of my thesis committee, Jinny Sisson and Bill Symes for their patience and understanding.

I would also like to thank the field crew of Rice personnel who collected the data, Ed Criley of the USGS, and IRIS/PASSCAL for the recording equipment. Special thanks go to Ralph Stegan of Phelps-Dodge for providing site support, geologic information, and patience in answering my many questions. A big thank you goes to Peeter Akerberg, my “partner-in-crime” on this project; thank you for your assistance, suggestions and support.

Finally, I would like to thank those that supported me in this effort. Thank you’s go to Jim and Beatrice for daily office support, and to my family for watching over me. Thanks also go to Phoenix, who always make sure I know what is important and to my mother who told me to go for it when the acceptance letter came.

This is dedicated to my father, who once located an undiscovered copper deposit with a gravimeter.

TABLE OF CONTENTS

	PAGE
INTRODUCTION	1
<i>Geologic Background</i>	5
METHODS	8
<i>Data Acquisition</i>	8
<i>Processing</i>	11
The Gila Line	11
The Bench Line	23
The Concentrator Line	38
INTERPRETATION	48
The Gila Line	48
The Bench Line	50
The Concentrator Line	56
DISCUSSION AND CONCLUSIONS	63
REFERENCES USED	69
List of Tables	
Table 1 – Data Acquisition Parameters	9
Table 2 – Processing flow for Gila Line, sledgehammer source data	23
Table 3 – Processing flow for the Bench Line	37
Table 4 – Processing flow for the Concentrator Line	47

List of Figures	PAGE
Figure 1 – Location Map	4
Figure 2 – Aerial View	4
Figure 3 – Location of seismic profiles	10
Figure 4 – Gila Line mine wall	12
Figure 5 – Gila Line stacking chart	13
Figure 6 – Gila Line amplitude spectra	14
Figure 7 – Sledgehammer processing sequence	15
Figure 8 – NMO – F-k technique on synthetic without noise	17
Figure 9 – NMO – F-k technique on synthetic with noise	18
Figure 10 – NMO – F-k technique on real data	19
Figure 11 – Gila Line CMP stack	21
Figure 12 – Depth migrated Gila Line image	21
Figure 13 – Depth migrated image with velocity model	22
Figure 14 – Bench Line mine wall	24
Figure 15 – Bench Line stacking chart	25
Figure 16 – Bench Line processing sequence	28
Figure 17 – Bench Line amplitude spectra (absolute)	29
Figure 18 – Bench Line amplitude spectra (normalized)	29
Figure 19 – Bench Line sledgehammer CMP stack	30
Figure 20 – Bench Line sledgehammer depth migrated	30
Figure 21 – Bench Line dynamite CMP stack	31

Figure 22 – Bench Line dynamite depth migrated	31
Figure 23 – Bench Line final velocity model	33
Figure 24 – Bench Line velocity model with depth migration	35
Figure 25 – Combined depth migrated section	36
Figure 26 – The Concentrator Line	39
Figure 27 – Concentrator Line stacking chart	40
Figure 28 – Absolute amplitude spectra	41
Figure 29 – Normalized amplitude spectra	41
Figure 30 – Concentrator Line processing sequence	42
Figure 31 – Concentrator Line CMP stack	44
Figure 32 – Concentrator Line filtered stack	44
Figure 33 – Concentrator Line time migrated	45
Figure 34 – Concentrator Line depth migrated	46
Figure 35 – Overlain on velocity model	46
Figure 36 – Gila Line with interpretation	49
Figure 37 – Gila Line photo with features marked	51
Figure 38 – Gila Line interpretation	51
Figure 39 – Bench Line with interpretation	54
Figure 40 – Bench Line photo with features marked	57
Figure 41 – Bench Line interpretation	57
Figure 42 – Concentrator Line with interpretation of time migration	58
Figure 43 – Concentrator Line with interpretation of time migration	59
Figure 44 – Concentrator Line close-up view	61

INTRODUCTION

In 1996, Rice University Department of Geology and Geophysics conducted a 2-D high-resolution seismic survey at the Phelps-Dodge Tyrone open pit copper porphyry mine in southwest New Mexico. Using multiple source types, several seismic profiles were conducted along the rim of the main mine pit and vicinity. The major objectives of this seismic study are to: Image the top of the crystalline bedrock at a meter scale; test whether ore bodies, or zones of mineralogic alteration within the bedrock, can be illuminated; and locate features that influence structure and groundwater flow in the near surface (less than 300 m depth). This document presents the results of three seismic lines shot outside and along the edge of the main pit. Two lines were located along the top of the main pit, a 500 meter long line on the southeast edge (referred to as the Gila Line) and a 400 meter line on the northeast wall (the Bench Line). A third line, the Concentrator Line (300 meters long), positioned outside the mine area, targeted an area of high-grade sulfides. Dynamite and sledgehammer sources were used for the Bench and Gila Lines, to provide seismic resolution in overlapping bandwidths (center frequencies of $40 \pm 30\text{Hz}$ for dynamite, $70 \pm 30\text{Hz}$ for Gila sledgehammer, $80 \pm 40\text{Hz}$ for Bench sledgehammer). The sledgehammer imaged the smaller scale features at the top of the mine and the dynamite provided data on the larger scale features deeper in the mine. By locating two of the lines along the rim of the mine pit, comparisons of the seismic results with photographs taken of the mine walls are possible. Features seen in these photographs can be correlated with those seen in the seismic sections. Coupled with

borehole information, this provides continuous geologic information for correlation along the entire length of the lines, an advantage not generally available to most seismic investigations.

Ongoing mine activity during data acquisition caused unusual environmental conditions with strong ambient noise from the operating equipment (drill rigs, steam shovels, ore trucks, and high voltage power lines). The removal of this noise was a major focus of the initial data processing. The resulting depth migrated images show the sedimentary overburden, the unconformity between the conglomerate and the crystalline rock, zones of mineralogic alteration within the crystalline basement, and near-surface features (fractures and depositional features of the sedimentary units).

Recent studies have employed seismic methods to image near subsurface features in crystalline rock (Kim et al., 1994), (Juhlin and Palm, 1999), (Adam et al., 1992) and within mines (Hill, 1992). In these studies, structural features (shear zones, unconformities) and lithologic changes were located using minimal data processing techniques. Later studies of laboratory measurements of massive sulfides and common host rock types (Salisbury et al., 1996) showed that varying with the grade of the ore, large sulfide deposits have high seismic impedance and thereby are good seismic reflectors. Milkereit et al. (1996) took the next step by conducting a high-resolution seismic survey across a massive sulfide deposit, validating the laboratory results, and demonstrating that seismic reflection methods are very useful for mapping massive

sulfide bodies. With this success, use of seismic reflection techniques for mining began (Adam et al., 1998, Adam, et al., 2000). Calvert and Li (1999) used seismic reflection methods to image the top of a sulfide deposit (800-1000 m. depth). Seismic reflection surveys, with the express purpose of locating massive sulfide deposits, are now accepted reconnaissance tools for the Canadian mining industry (Adam et al., 2000). 2-D and 3-D seismic surveys have also been used as reconnaissance tools to locate gold deposits in South Africa (Stuart et al., 2000), (Gibson et al., 2000).

The Phelps-Dodge Tyrone porphyry copper mine is located in Southwest New Mexico in the Burro Mountain mining district and is situated near the town of Tyrone (Figure 1). The mine is an open pit operation, started in 1969. Low grade copper ore, less than one percent for every ton of extracted material, is removed from the mine pit (Kolessar, 1982). By 1999, 160 million pounds of copper had been extracted (Phelps-Dodge: <http://www.phelpsdodge.com/index-pduc.html>). Reconnaissance of the ore body is conducted using a grid of boreholes spaced 200 feet apart and each 1000 feet deep. The cost is high for these boreholes, approximately 25 dollars a foot or \$25000 per drill hole (Stegan, pers. comm., 1998). The successful deployment of seismic reflection surveys would allow for the grid spacing to be increased, reducing the costs, with the reflection data “linking” the boreholes by providing a continuous picture of the subsurface. Beyond imaging ore deposits, near-surface seismic surveys could potentially locate structural features such as faults and fracture zones that could cause excavation problems and influence groundwater flow.

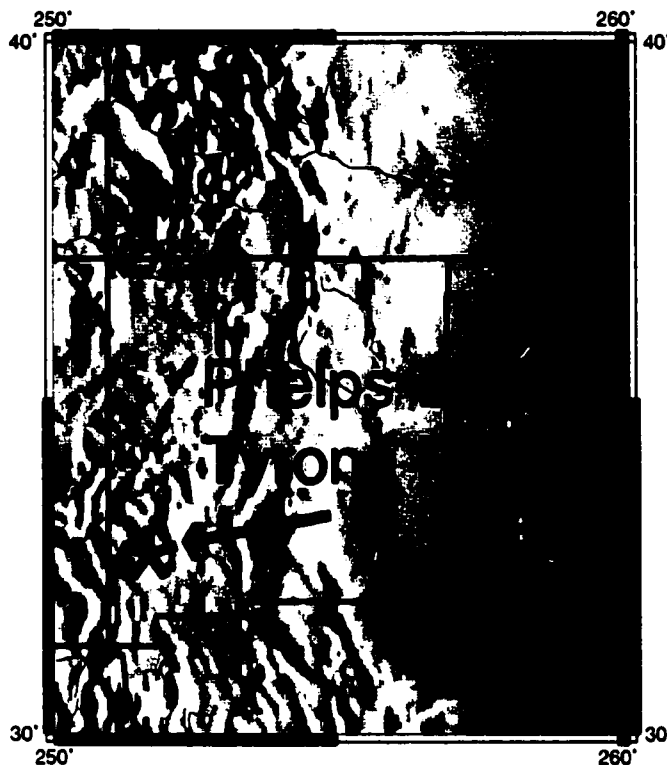


Figure 1 - The Phelps-Dodge Tyrone open pit porphyry copper mine is located in southwest New Mexico.

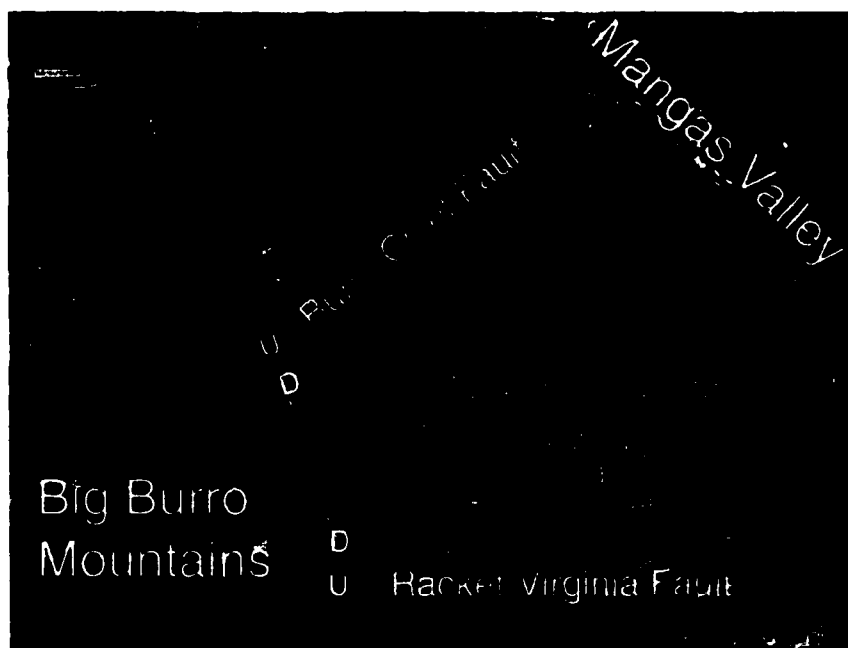


Figure 2 - Aerial photo of the Phelps-Dodge Tyrone mine within the Burro Mountain District. The mine extends over seven square kilometers in area. Approximate location of faults described in the text are based on DuHamel et al (1995). This photo is adapted from a USGS photo (9/28/1996).

Geologic Background

The Phelps-Dodge Tyrone mine is located within the southeast portion of the Basin and Range Province. The mine is on the west edge of the Mangas Valley which trends northwest southeast, with the Little Burro Mountains on the east edge of the valley. The Big Burro Mountains to the west (Figure 2) are primarily of Precambrian granodiorite. The mine, itself, is in the northeast portion of the Tyrone Stock, quartz monzonite porphyry, Laramide in age (56.2 Ma) intruded into the Burro Mountain granodiorite. The Tyrone Stock is bound by normal faults to the northwest and the southeast, forming a regional horst (DuHamel et al., 1995). Within the stock, the Burro Chief Fault on the west, and the Racket-Virginia Fault on the south, separate the northeast tip of the stock from the main body. Within the graben formed by the two faults, the bulk of the Tyrone Mine is located, (DuHamel et al., 1995).

Although categorized as a stock from gravity and magnetic data, the Tyrone Stock consists primarily of porphyries forming dikes and laccolithic intrusions within the host rock. The types of intrusives include porphyritic diorite, and porphyritic biotite dacite, biotite granodiorite-tonalite, intrusive breccias and porphyritic dacite. The different rock types reflect the timing of the intrusion with hydrothermal activity and later formation of intrusive breccias (DuHamel et al., 1995).

Overlying the crystalline rock is the Miocene Mangas Conglomerate (DuHamel et al., 1995), consisting of interbedded and weakly consolidated gravel, sand and tuff up to 600

m thick in the region, and 130 m thick in the mine (Page, 1922). Known regionally as the Gila Conglomerate, it overlies the entire mine, dipping 15-20 degrees to the northeast. Pleistocene and Quaternary age alluvium are also present in some places in the mine vicinity (DuHamel et al., 1995). Overlying the conglomerate in portions of the mine is a variable thickness of mine waste (tailings), referred to here as “stockpile”.

The Tyrone copper deposit is a result of the intrusion and related hydrothermal alteration of the host rock. The ore mineral, in this case chalcocite, occurs as interwoven veinlets throughout the host rock. The chalcocite appears as a coating on pyrite mineralization. The ore also deposited along faults and fractures and in breccias. The faults provided pathways for magma and hydrothermal activity, and as well, movement along the faults offset ore bodies. The higher permeability of the breccias allowed the hydrothermal solutions to saturate the breccias, resulting in higher concentrations of copper within this unit. The area below the Bench Line of this study includes a breccia that contains the highest grade ore in the mine (DuHamel et al., 1995).

Supergene enrichment altered the near surface mineral deposit, most likely as a byproduct of groundwater flow. Oxidation enriched the near surface deposits, creating acidic solutions that leached out the metals in the rock. These heavy sulfide metals sunk and reprecipitated, thereby enriching the minerals already present (Bates and Jackson, 1987). The enriched layer ranges from a meter to over 100 meters thick. Although the surface of the layer varies in depth, the general trend correlates with topography

(DuHamel et al., 1995). This enriched layer, containing up to one percent chalcocite, is a major target for the mining operation.

METHODS

Data Acquisition

We conducted three seismic profiles in the Phelps-Dodge Tyrone mine to investigate the suitability of seismic reflection methods to image the lithology and structure of the near-surface environment to a depth of 300 meters (m). The three seismic lines of the survey referred to as: The Gila Line, named for the Gila Conglomerate, called the Mangas Conglomerate within the mine and referred as such by this document. The Bench Line, named for the northern portion of the mine where it is situated, occurs over a topographic high, or bench, carved out by the mining process. Finally, the Concentrator Line, named for its proximity to the Concentrator building, is along the edge of a terrace just north of the mine pit. Figure 3 shows the location of each line on an aerial photo of the mine. Both the Gila and Bench lines follow the edge of the main pit of the mine. Dynamite and sledgehammer sources were used to target both the near surface shallow fine scale structures, and deeper large scale structures. The combination of both source types allowed us to image the entire depth of the mine (260-300 m).

The survey parameters for the seismic lines discussed in this paper are given in Table 1. A sixty channel recording system was used to record each source type with the system's acquisition filter set to reduce low frequency noise. The sample rate was set at one millisecond (ms) for both sources; however, the sample rate was reduced to 0.5 ms for the Concentrator Line. Receiver spacing of 2.5 m was used for all of the survey, but the

source spacing changed on the Bench Line from 5 m to 2.5 m for the sledgehammer.

Offsets varied with seismic profile and source type. Long offsets recorded for dynamite data on the Gila and Bench Lines were not possible for the Concentrator Line because of the limited area available at that location. The shooting configuration for each source type differed. Dynamite shooting occurred with the source kept at one end of the receivers in an “off-end” spread, unless the receivers were kept in place and then the source rolled through the receiver spread, resulting in a split spread. For the Gila Line, dynamite shooting and sledgehammer acquisition maintained a centered split spread through the profile. The processing portion of this document includes stacking charts for each of the lines.

	Gila Line	Bench Line	Concentrator Line
Sources Used	Sledgehammer (9kg) 10 hammer blows stacked per record	Dynamite (2kg at 3 m depth) / sledgehammer (9kg)	Dynamite (2 kg at 3 m depth)
Recording System	Bison 2460 60 channel 24 bit recording unit using sixty 28 Hz single component geophones. Geometrics Strataview 60 channel 24 bit recording unit using sixty 40 Hz geophones used for transmission data		
Acquisition filter	32 Hz to Nyquist		
Sample rate	1 ms	1 ms	0.5 ms
Receiver Spacing	2.5 m		
Shot Spacing	5.0 m	5.0 / 2.5 m	5.0 m
Typical Offsets	2.5 – 75 m	150-300 / 2.5-75 m	2.5-150 m
CMP Spacing	1.25 m		
Ave Fold	20	15 / 20	15
Length of seismic line	300 m of 500 total length	400 m	300 m
Spread	centered split	off end / centered split	off end / split spread
Bandwidth	40-90 Hz	10-65 / 40-120 Hz	12-65 Hz
Number of source gathers	43	71 / 148	47

Table 1 – Data Acquisition Parameters

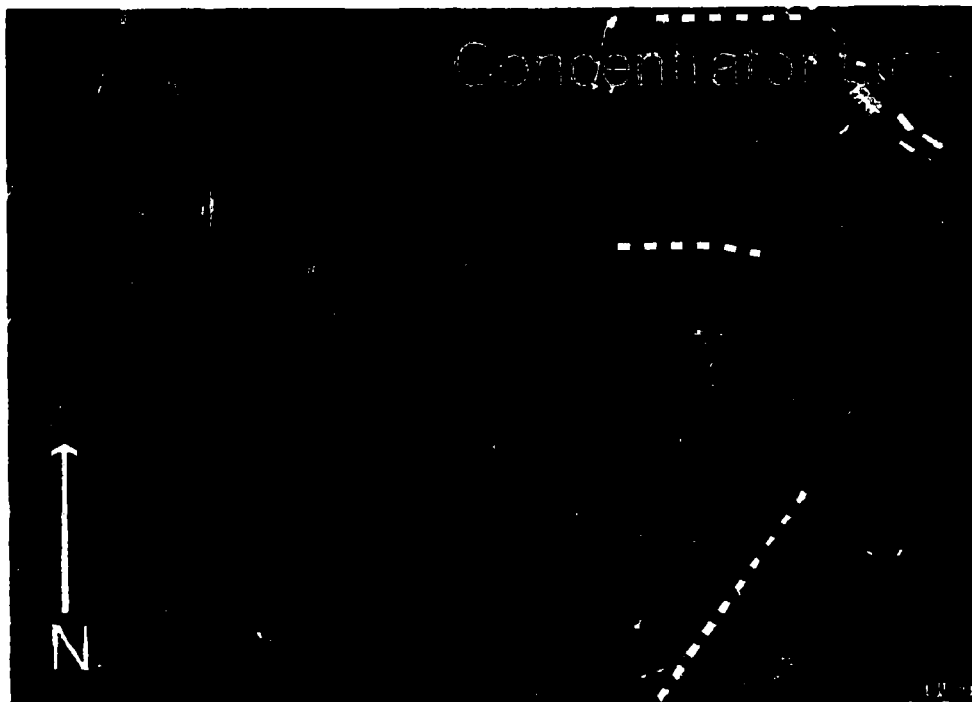


Figure 3 - An aerial view of the mine showing the location of each seismic profile of the survey (USGS, 28/9/1996). The main pit is approximately 3 square kilometers in size. The illumination is from the southeast, casting heavy shadows over the southeast edge of the pit.

Processing

The Gila Line

For the Gila Line (Figure 4), data were collected using a nine kilogram sledgehammer along the western 300 meters of the 500 m line. At every source location, ten hits of the sledgehammer on a metal plate were stacked into a single shot gather. Data collection and processing of the dynamite portion of the line is discussed in Akerberg (1999).

Figure 5 is a stacking chart showing source coverage and fold. Examination of common midpoint gathers (CMPs) from the raw sledgehammer data showed spatial aliasing resulting from the large (6 m) trace spacing caused by the 5 m source offset. To avoid the aliasing, processing for the entire survey was done in the shot and receiver gather domains (2.5 m trace spacing) to maintain signal symmetry. For the Gila sledgehammer data, however, signal strength was not strong enough to repeat the filtering process in receiver gathers. Figure 6 shows absolute and normalized amplitude spectra for a sledgehammer source point along the Gila Line. Table 2 summarizes the processing sequence.

Strong ambient noise from ongoing mine operations was a major concern, the mine noise from trucks and excavation equipment dominating the sledgehammer signal (Figure 7a). Initial data conditioning included trace editing, and muting out environmental noise at times less than the direct arrival. An inside mute was applied later in the processing sequence to remove source noise (hammer bounces). A Butterworth bandpass filter with a pass band of 60 – 120 Hz was used to remove low frequency and 60 Hz mining

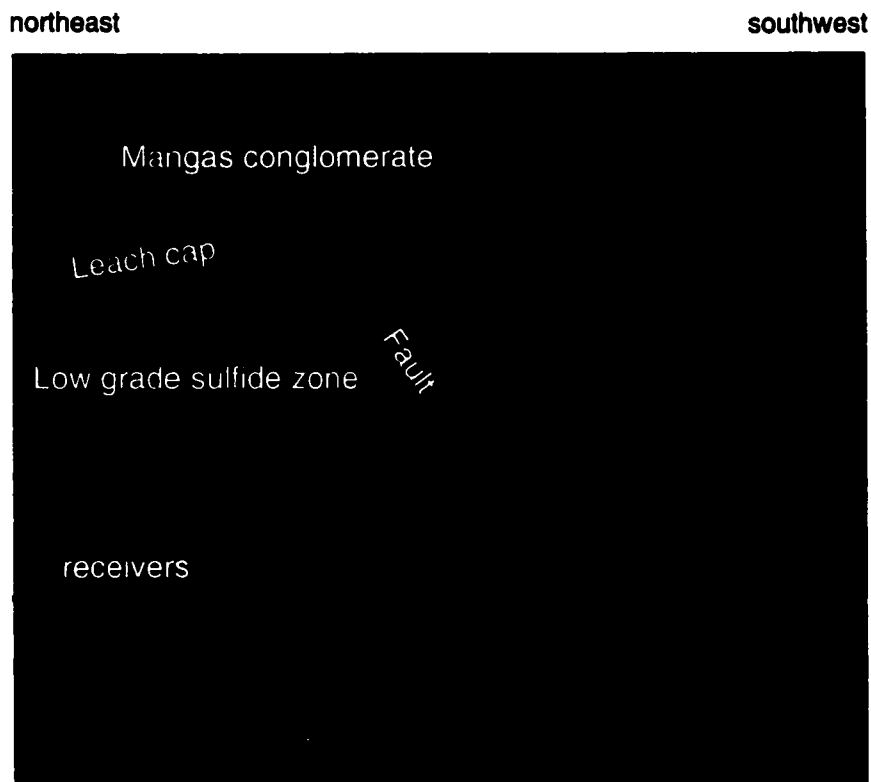


Figure 4 - The mine wall below the Gila Line. Each bench is 15 m high, making a total depth to the mine floor of 300 m. Geology from mine information and that seen on the wall face is labeled. The unconformity below the Mangas (green line) is seen in the photograph, as is the fault and the leach cap. The low grade sulfide zone is inferred from borehole information. The receivers shown at the lower left in the picture were used to collect transmission data that was used in the calculation of a velocity model for migration (Akerberg, 1999).

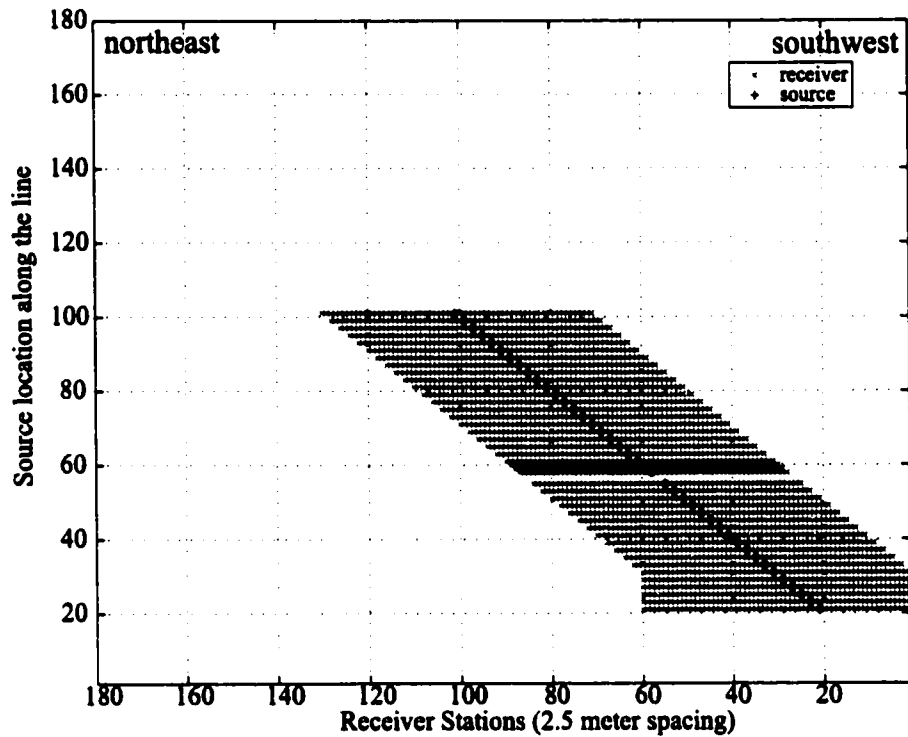


Figure 5 - Stacking chart for Gila Line sledge hammer source data. Sledgehammer data were collected over 300 m of the 500 m survey profile. The source spacing was 5 m over the majority of the line, placed at every other receiver station. For comparison with the picture of the mine wall (Figure 4), receiver station one is at the southwest end of the line.

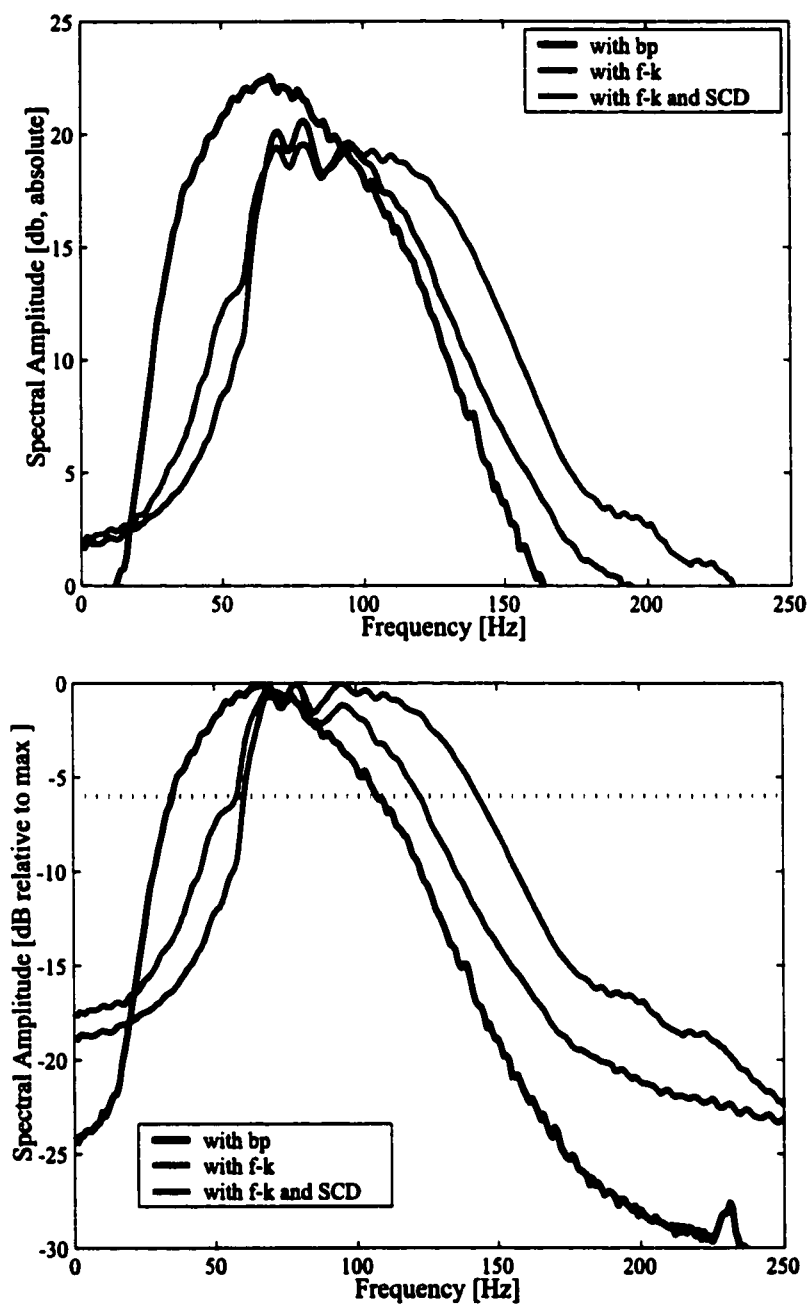


Figure 6 - Gila sledge hammer amplitude spectra for source pt. 60. The blue line shows the amplitude spectra of a single shot with the bandpass filter (bp) applied. The red line shows a source spectra further into the processing sequence, after the F- k filter has been applied removing the low frequency noise. The green line shows the spectra after applying surface constant deconvolution (SCD).

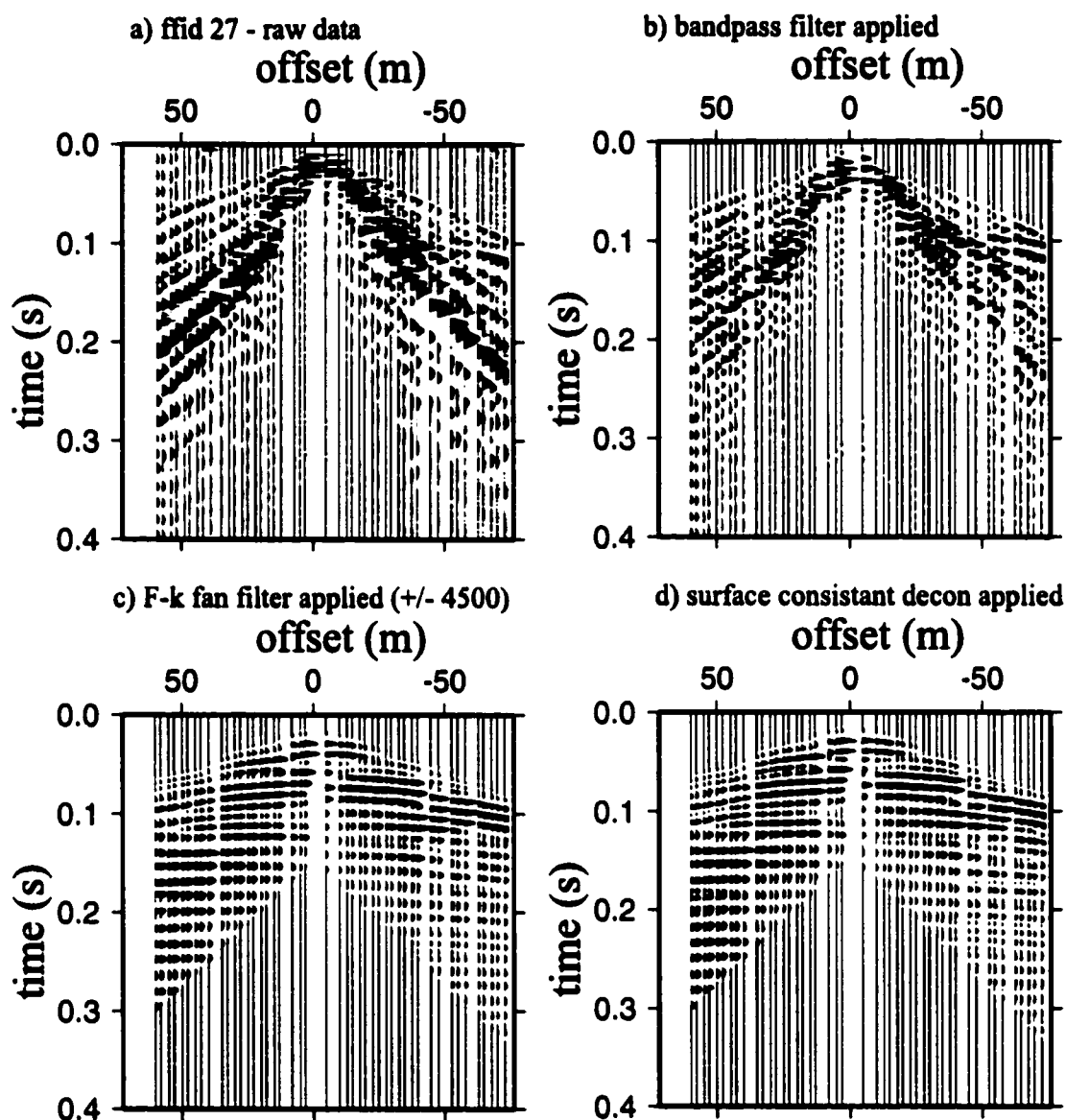


Figure 7 - A single sledgehammer source gather illustrating the processing sequence for the Gila Line (Table 2). Figure (a) shows the raw data, with strong linear noise dominating the gather. Figure (b) shows the same gather after application of the bandpass filter. The linear noise is reduced, but is still predominant in the gather. Figure (c) is the gather after application of the F- k filter. The linear noise has been removed, but the gather is ringy. Figure (d) shows the gather after surface constant deconvolution and a bottom mute.

equipment noise (Figure 7b). The filtered shot gathers show strong organized noise in the form of groundroll and refractions that mask the weaker reflections. Ideally in seismic reflection surveys, a survey is designed with groups of geophones deployed to filter groundroll. High-resolution surveying commonly does not employ geophone groups, requiring that ground roll be either frequency-wave number (F-k) filtered or muted. When survey design does not prevent recording of groundroll, it is often muted from the data set. In this case, an F-k filter was applied because the groundroll is fast enough that muting would reduce the range of offsets available for stacking, which would severely limit the depth and reduce the near-surface coverage of the seismic image.

In order to divide groundroll and refractions from reflections and preserve the complete offset range, a normal moveout correction (NMO) was used to flatten reflections by temporarily increasing their apparent velocity. With this increase, the reflections are separated from the much lower velocity groundroll and refractions and this separation is readily apparent when viewing the gathers in the F-k domain. Applying a high velocity F-k fan filter that retained velocities larger than ± 4500 m/s removed the lower velocity noise. By applying an inverse NMO correction (INMO), the filtered output returned to the original alignment. Figure 8 illustrates this process on a synthetic gather without added noise. Figure 9 shows the process with heavy white noise superimposed on the signal. Finally, Figure 10 shows the effect of the NMO-F-k-INMO process on source gather 13. In each case, the process removes the linear events, leaving the hyperbolic reflections. Surface consistent deconvolution followed, removing ringiness in the data

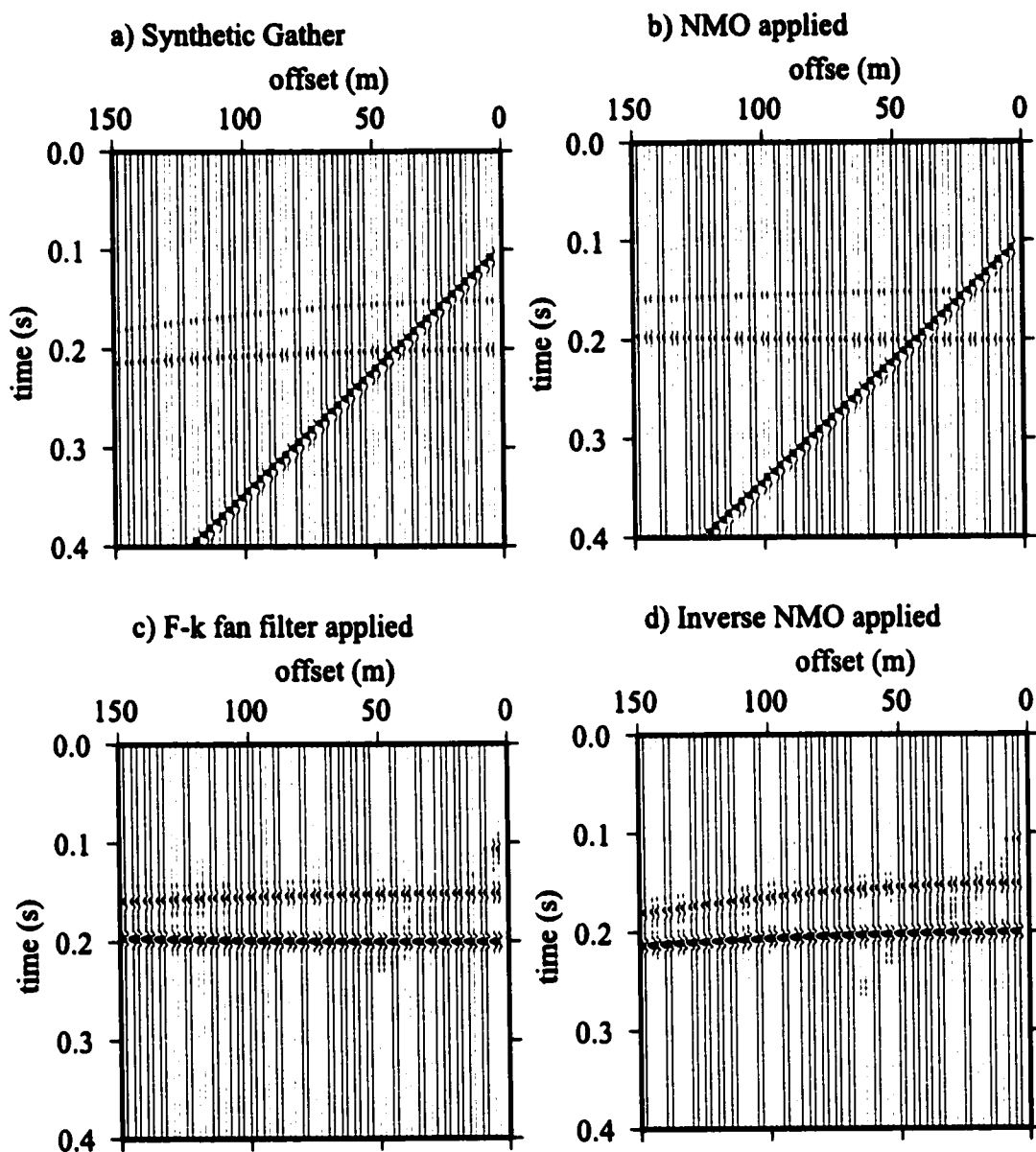


Figure 8 - NMO - F-k Fan Filter - Inverse NMO Technique shown on synthetic source gather without noise. The gather shows two weak reflections and one strong linear event. Figure (a) shows the gather before processing. Figure (b) shows it after NMO was applied, flattening the reflections. Figure (c) is the gather after the F- k filter was applied, having removed the linear event. Figure (d) shows the gather after inverse NMO was applied, returning the reflections to their original form.

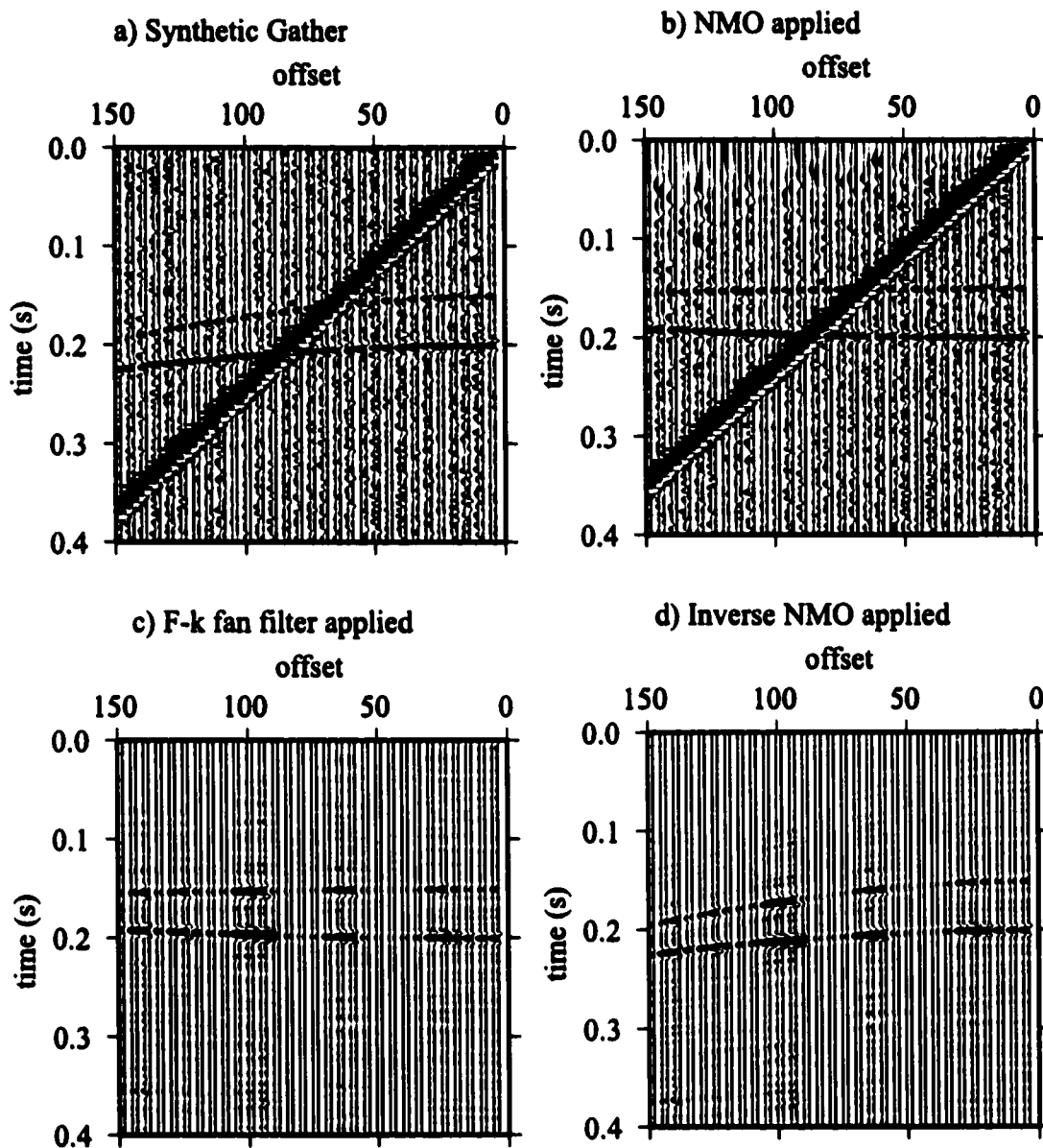


Figure 9 - NMO - F-k Fan Filter - Inverse NMO Technique using a synthetic source gather with added random noise. The same processing sequence as shown in Figure 8 but with strong noise dominating the gather.

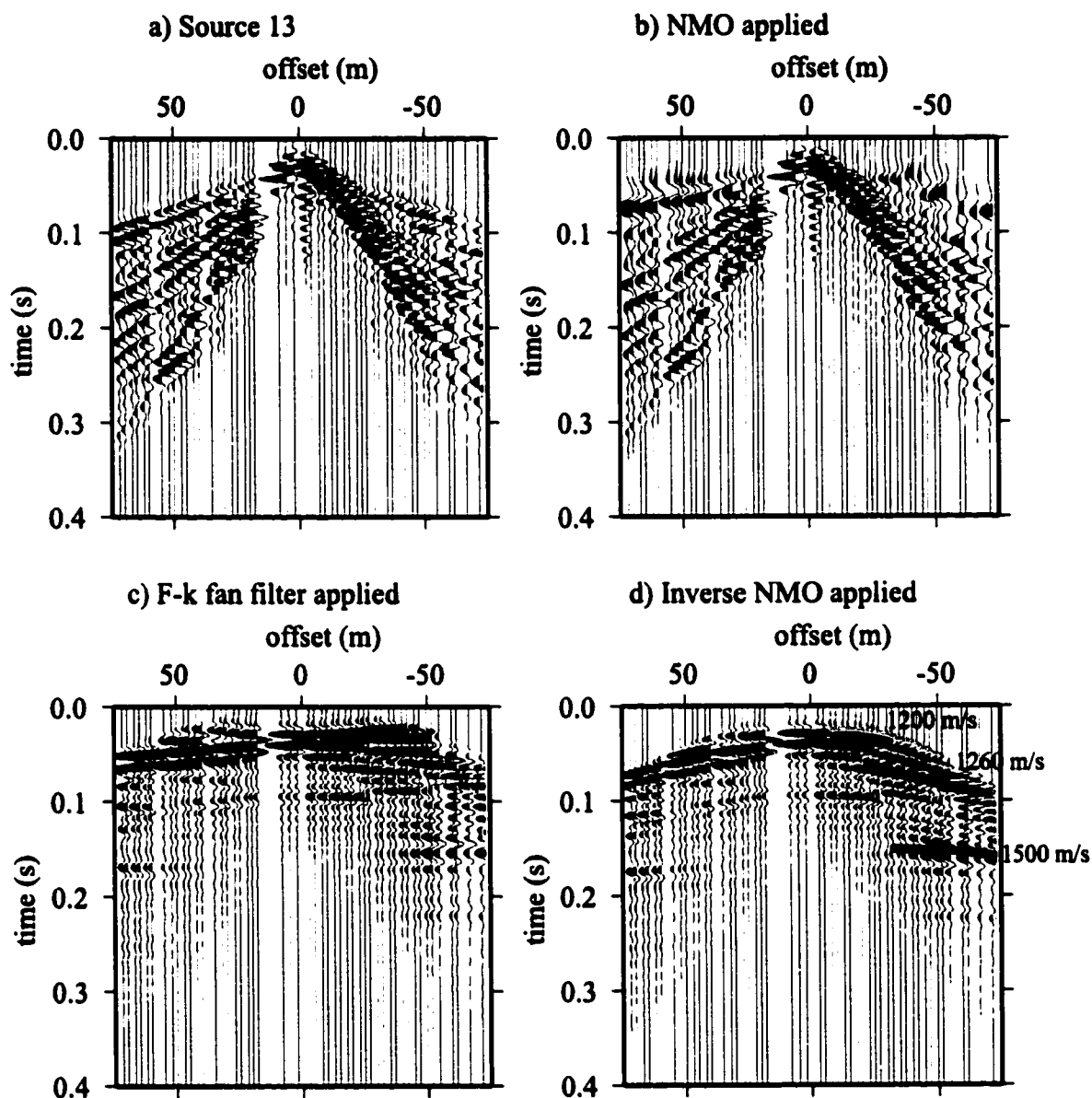


Figure 10 - NMO - F-k Fan Filter - Inverse NMO Technique applied to a Gila Line sledgehammer source gather. Figures 8 and 9 demonstrate the process on synthetic data.

caused by the application of the narrow F-k filter. Figure 7a-d demonstrates the step-by-step effect of the entire data processing flow.

Velocity analysis consisted of two steps: First, constant velocity stacks (CVS) were made across a range of velocities (900-2500). The initial velocity model was refined using semblance analysis followed by semblance analysis and stacking analysis in combination, conducted on the filtered data determined adequate stacking velocities for the section. The stacking velocity model for the hammer data set varies from 1100 to 2350 m/s. Data were then NMO corrected and stacked. Figure 11 is the final common midpoint (CMP) stack with a nominal 20 trace fold.

Post stack depth migration was performed using a migration velocity model developed by Akerberg (1999) as part of his analysis of the dynamite portion of the Gila Line. He utilized travel time inversion of dynamite and sledgehammer source first arrival times to construct a interval velocity model (in depth). The velocity model constrains velocities for the sedimentary layer from 700 to 2500 m/s. Figure 12 shows the depth migrated sledgehammer stack and Figure 13 shows it overlain on the velocity model. As a quality check, post stack time migration using smoothed stacking velocities resulted in a migrated image that supports the depth migration results.

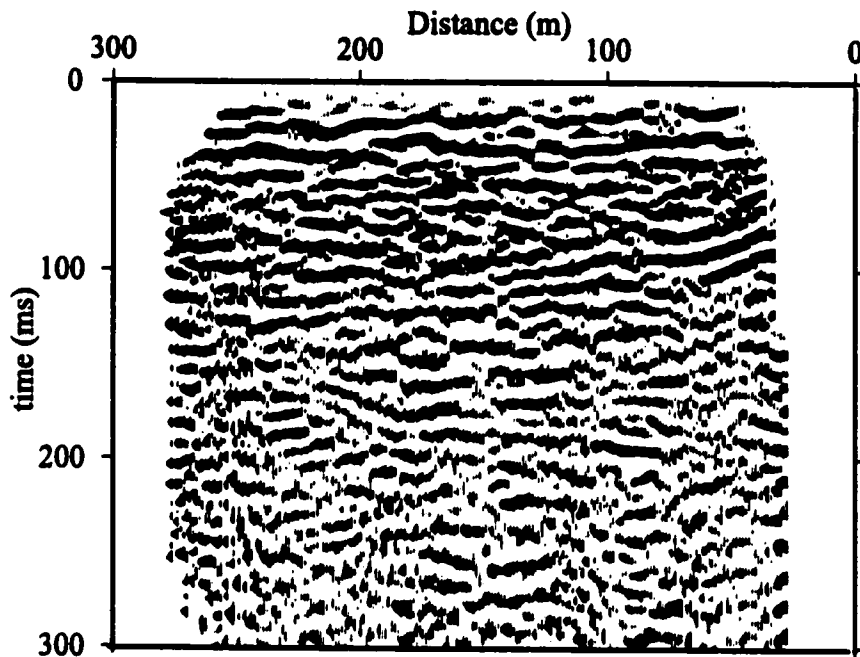


Figure 11 - Gila Line CMP stack of sledge hammer data.

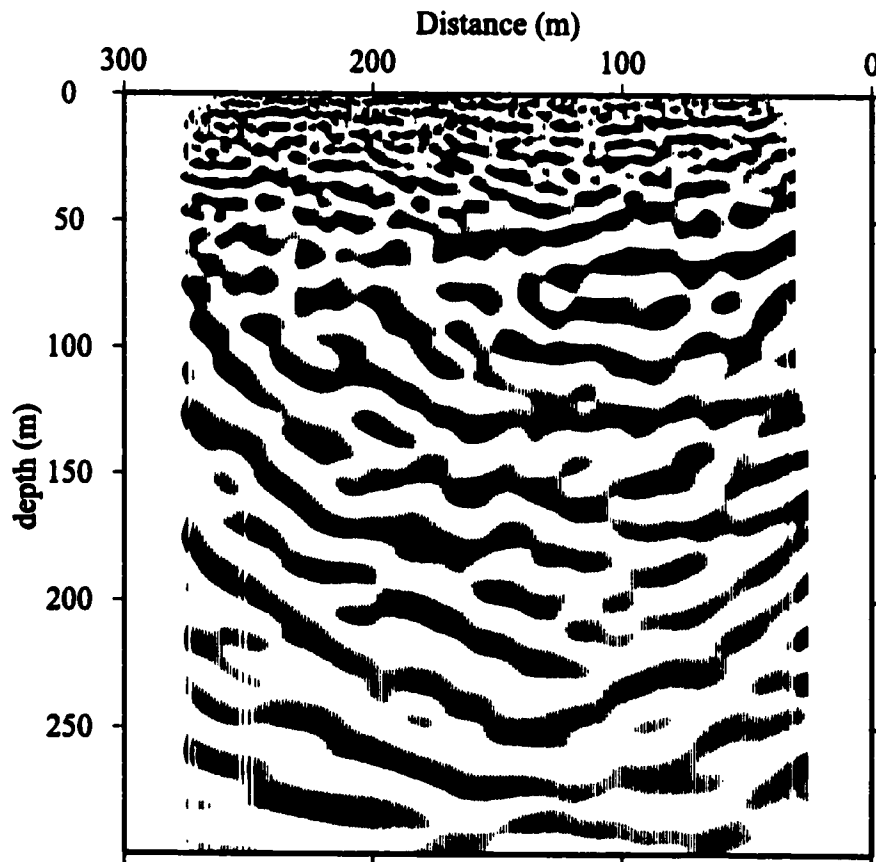


Figure 12 - Depth migrated CMP stack of sledge hammer data. The velocity model used for the migration was smoothed and scaled at 90 percent of the velocity model developed by travelttime analysis (Figure 13).

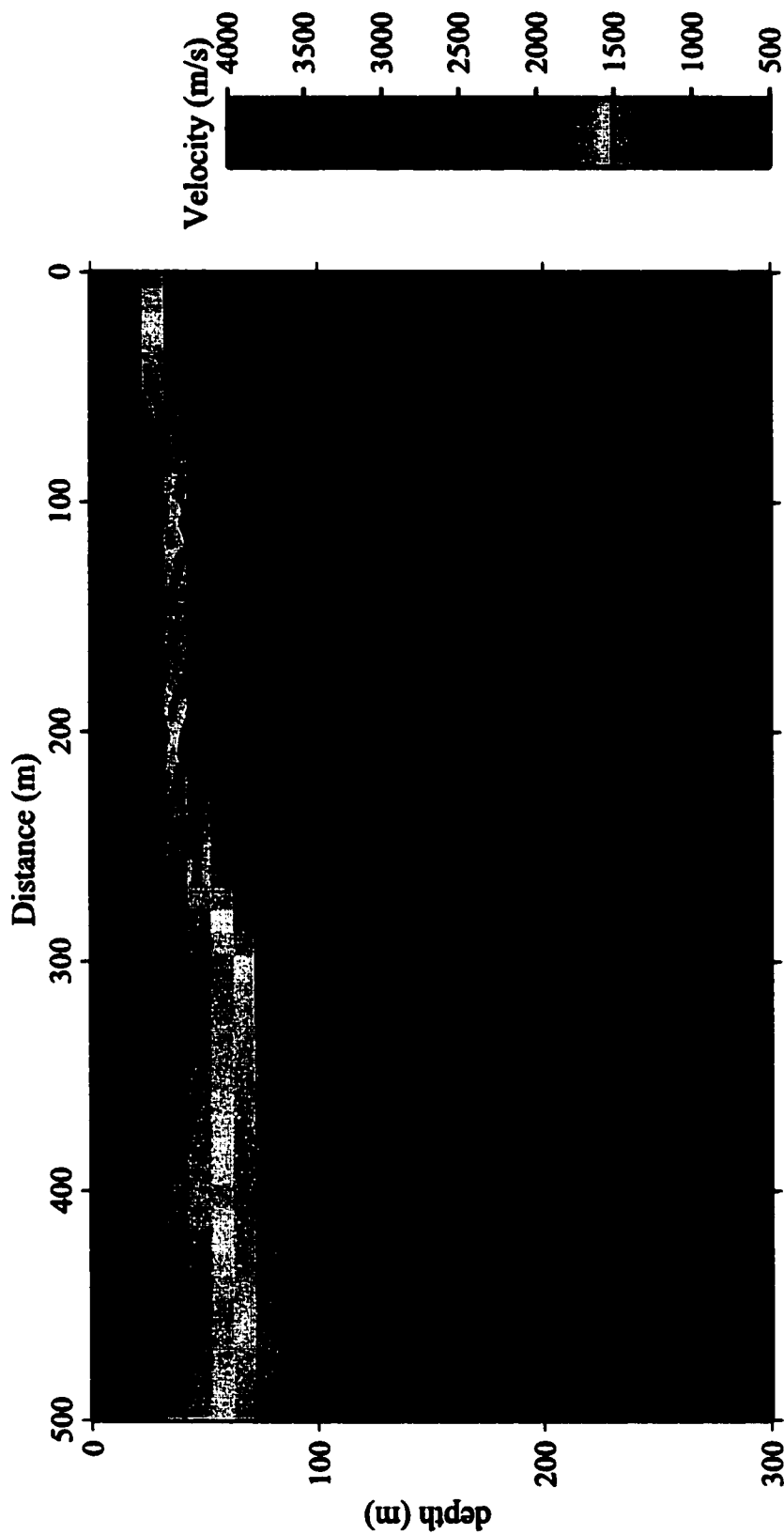


Figure 13 -- Gila Line depth migrated combined source section overlain on the velocity model. The velocity model was developed using both sledgehammer and dynamite first break information from receivers at the top of the mine, and from receivers placed at the bottom of the mine to collect transmission data. The sharp change in velocity correlates to the unconformity between the slower sedimentary units over the crystalline basement. The velocity contrast below 100 m depth correlates to a fault within the mine wall (figure adapted from Akerberg, 1999).

Trace Editing (kills/reversals)
Trace DC Removal
Elevation Statics
Top Mute
Bandpass Filter (Butterworth 60-120 with -18 and -36 dB/octave slopes)
Velocity Analysis
NMO Applied (for F-k application only)
F-k Filter (fan filter of +/- 4500 m/s from 60-120 Hz)
NMO Removed
Surface Consistent Deconvolution
Trace Equalization
Bottom Mute
Velocity Analysis (CVS followed by semblance analysis)
NMO applied
CMP Stack
Kirchhoff Depth Migration (using velocity model from travelttime analysis)

Table 2 – Processing flow for Gila Line, sledgehammer source data.

The Bench Line

The Bench Line (Figure 14) has the highest levels of ambient noise in its shot records. Operation of mine excavation equipment located below the profile and adjacent to the east end of the profile (the equipment can be seen in Figure 14) during data collection contaminated sledgehammer and dynamite source gathers. Figure 15 is a stacking chart showing the fold and configuration of the seismic line. The noise is most obvious in the sledgehammer records with small shot receiver offset. Although the linear noise is not as obvious in the dynamite records with large source receiver offset (150 m minimum), the same processing sequence to reduce groundroll and linear noise was applied to both data sets. Table 3 details the data processing flows for both source types. Spatial aliasing seen in the CMP gathers was less prevalent in the sledgehammer source records. All data

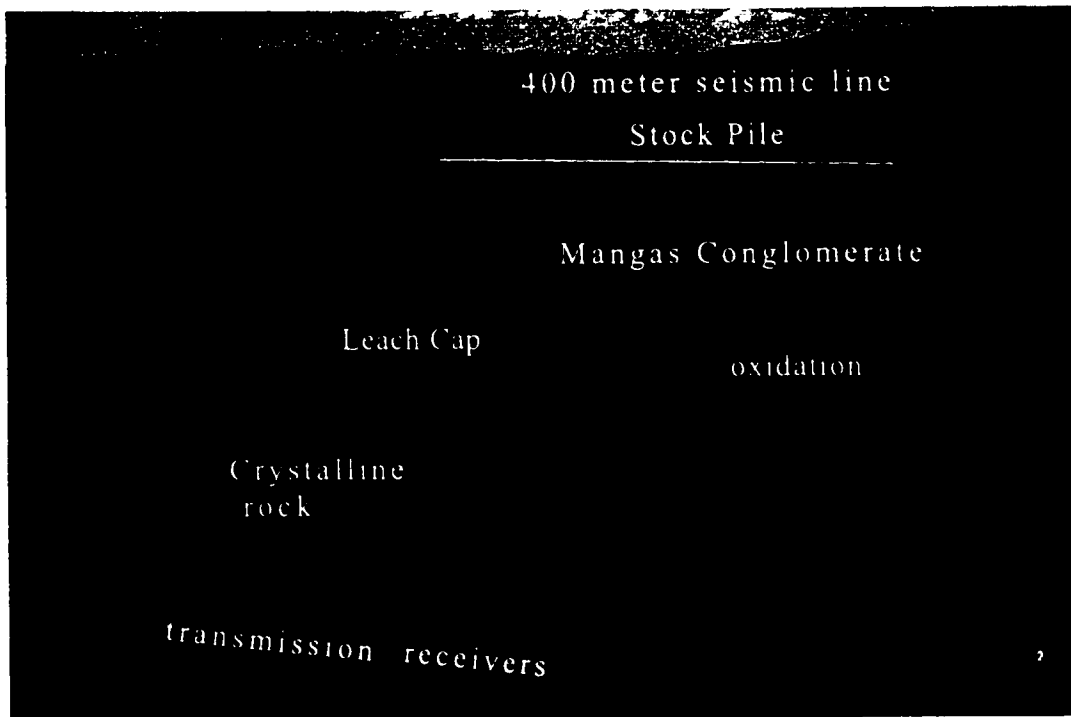


Figure 14 - The mine wall underlying the Bench Line. The major rock types are labeled. The stockpile, Mangas Conglomerate and oxidized zone are all visible on the photograph. Individual units are not discernable below the unconformity. The leach cap and lower units are inferred from borehole data. The data from the transmission receivers was not used for this line. Most of the gathers suffered from timing problems and the array was not situated deep enough to be of significant use in developing a velocity model for this line. Each bench is approximately 15 m high. The mine wall is 260 m in height. Mine excavation equipment, in operation during data collection, is visible below and to the east of the profile.

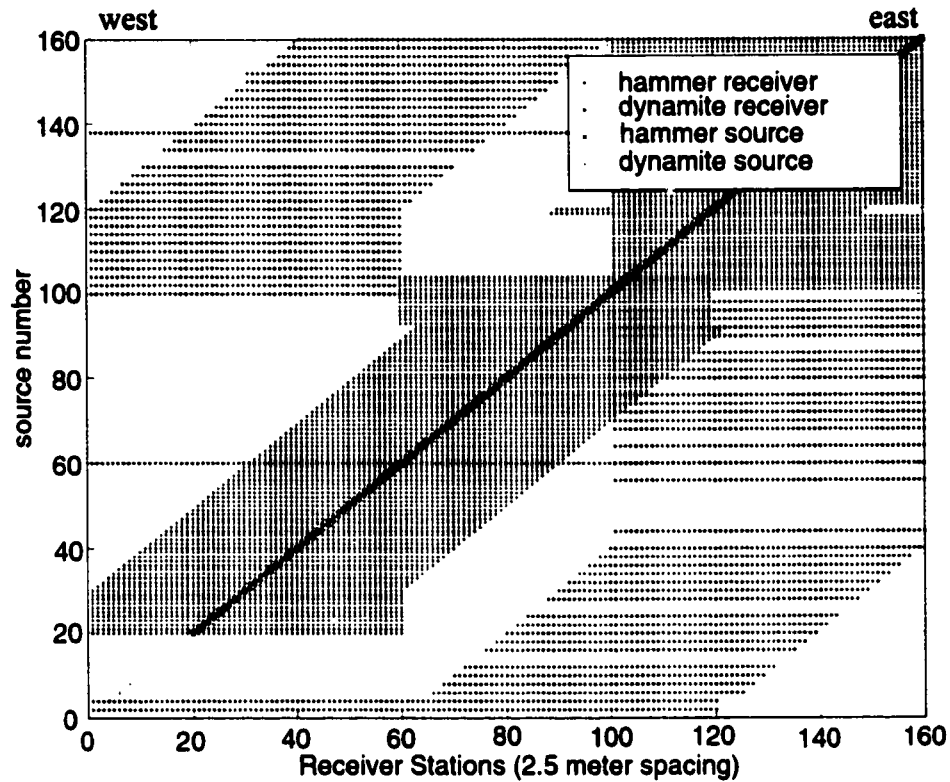


Figure 15 - Stacking chart for the Bench Line. Dynamite is in blue and sledge hammer receiver locations are in green. The source spacing for the sledge hammer was 2.5 m and 5.0 m for dynamite. Neither source type covers the entire extent of the line. Dynamite source data covers the western 330 m of the 400 m line. Sledgehammer data covers the eastern 380 m.

conditioning utilized source gathers, and when necessary, filtering (velocity filtering) was repeated in receiver gathers.

Following trace editing, static corrections were applied to the data to correct a timing error for several dynamite source gathers. To reduce environmental noise, Butterworth bandpass filters, one with corners at 50 and 183 Hz for the sledgehammer data and another with corners at 20 and 140 Hz for dynamite data, were designed using filter panels. Application of a notch filter at 120 Hz removed the harmonic from the 60 Hz noise from mine operations. A large amount of coherent linear noise remained in the data. To reduce this noise, trace mixing was applied along the measured apparent velocities of the linear events (331 and 271 m/s for sledgehammer, 345 m/s for dynamite). Eleven traces were used to flatten the data to the specific velocity before calculating a mixed trace. The mixed trace, in this case a median trace, was used as a calculated filter and subtracted from the data, removing the large amplitude linear events from the gathers.

A tau-p (τ -p) transform filter applied to the data removed the remaining low velocity coherent noise, keeping the higher velocity signal. A velocity filter, the τ -p filter transforms the data from time and offset domain to tau (intercept time) and p (slowness) using the Radon Transform. Use of the transform allowed me to avoid both the single offset limitation of the F-k filter module encountered during processing of the Gila Line, and noise at near zero offsets and at gather edges (both spatial and temporal) from the filter (Yilmaz, 1987). Trace spacing is a constant 2.5 m in source gathers, however, trace

spacing is variable within receiver gathers and can vary from 2.5 m up to 100 m. Each of these offsets must be F-k filtered separately and then ‘knitted back together’ to reform the receiver gather. By specifying a limited transform window (± 1000 ms/km), low velocity events were not included in the gather after reapplication of the filter to transform back to the distance – time (x-t) domain. Application of surface consistent deconvolution reduced ringiness in the data from filtering. Lastly, application of a top mute removed filter artifacts and a bandpass filter removed high frequency artifacts from deconvolution. A bottom mute was also applied to the sledgehammer data to remove noise from hammer bounces. Figure 16 illustrates the effect of the processing flow on both source types.

Figures 17 and 18 show the amplitude spectra for both source types early in the processing sequence, and at the end. The absolute amplitude plot (Figure 17) shows the much stronger dynamite signal over the weaker sledgehammer. When viewed as normalized values (Figure 18), the bandwidth of the sledgehammer (40-120 Hz, or 1.5 octaves) is also less than the dynamite (15-60 Hz, or 2 octaves).

Starting with CVS velocity models, both semblance analysis and stacking velocity analysis of both data sets produced velocity models. The CMP stacks for the sledgehammer and dynamite data are Figure 19 and Figure 21 respectively.

Travel time inversion was used to construct a velocity model for post-stack Kirchhoff depth migration. Input to the inversion process, first break picks from 179 dynamite and sledgehammer source gathers. The travel time inversion code of Zelt and Smith (1992)

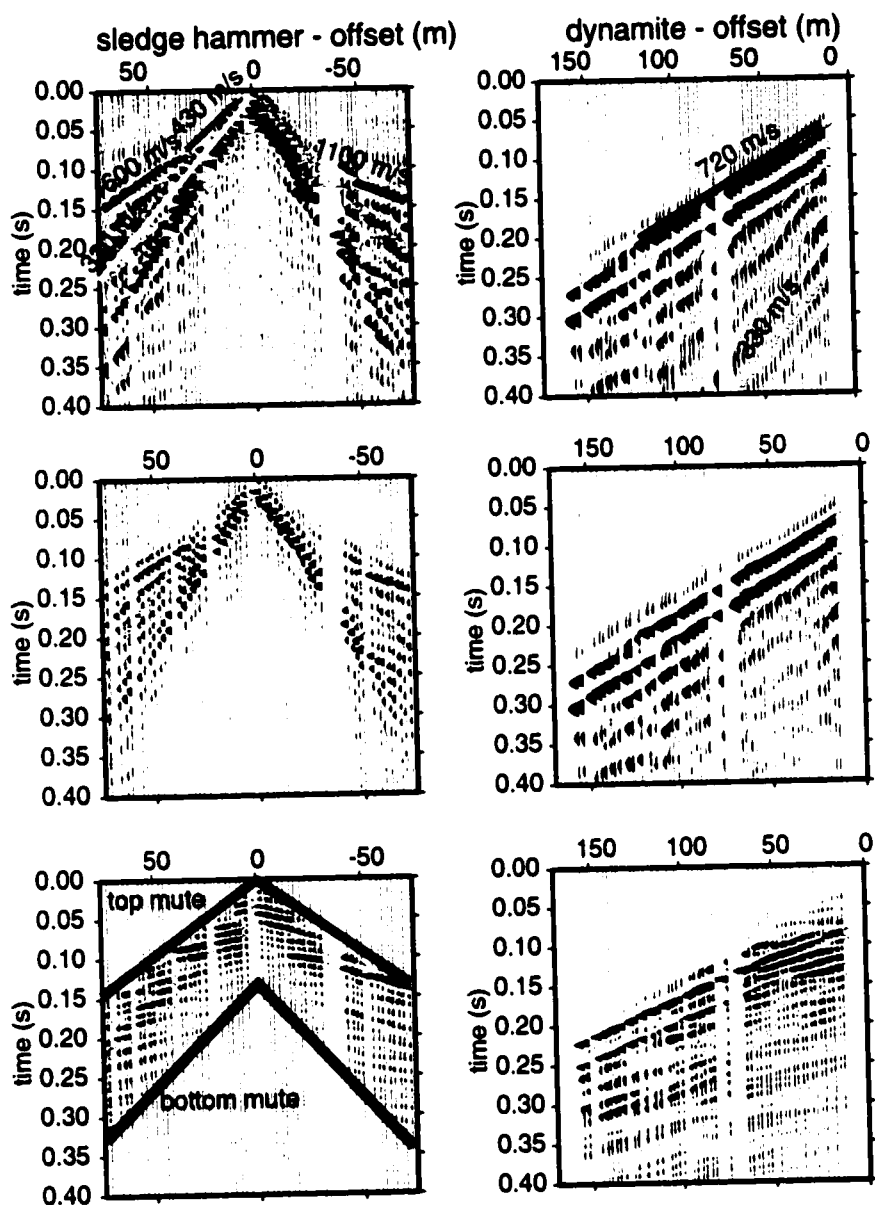


Figure 16 - Sledgehammer (left) and dynamite (right) source gathers shown step-by-step through the processing flow. Raw data are shown at the top, bandpass filtered data in the middle, and data with a bandpass filter, surface constant deconvolution and τ - p filter are at the bottom. Top and bottom mutes are shown for the sledgehammer data to remove artifacts from the filtering process and noise inherent in the data itself.

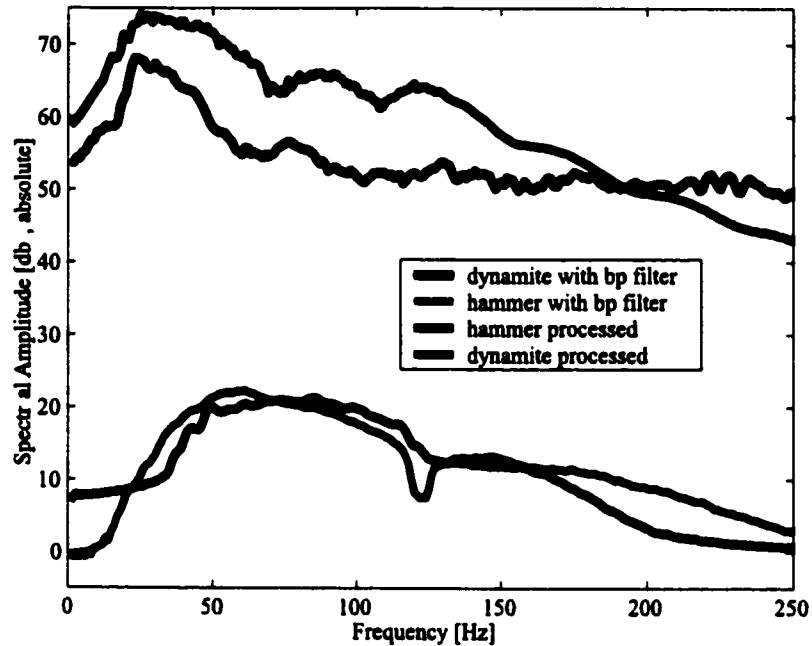


Figure 17 - Amplitude spectra for both source types after implementation of the bandpass filter and after the rest of the processing (Table 3) for a single source gather (source location 60) along the profile. The dynamite data has higher amplitude and wider bandwidth than the sledgehammer spectra.

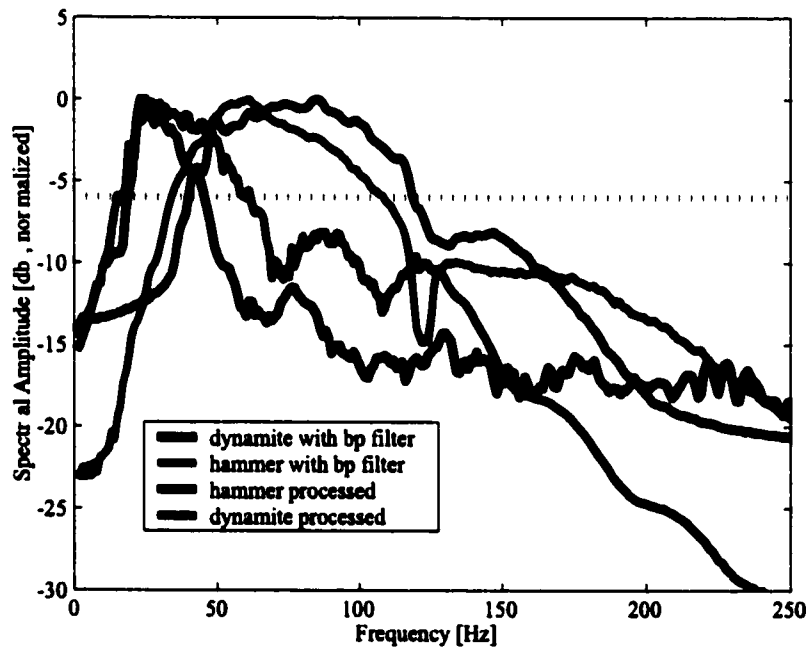


Figure 18 - Normalized spectra for both source types after implementation of the bandpass filter and after the rest of the processing (Table 3) for a single source gather (source gather 60) along the profile. The effect of the processing is visible by the wider main lobe of the processed data than the spectra with only the bandpass filter.

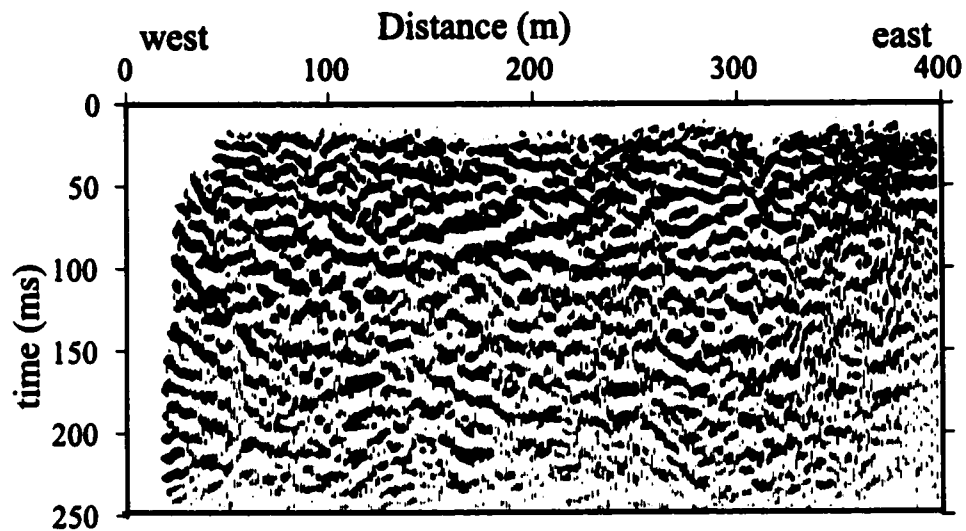


Figure 19 - CMP stack of Bench Line sledgehammer data.

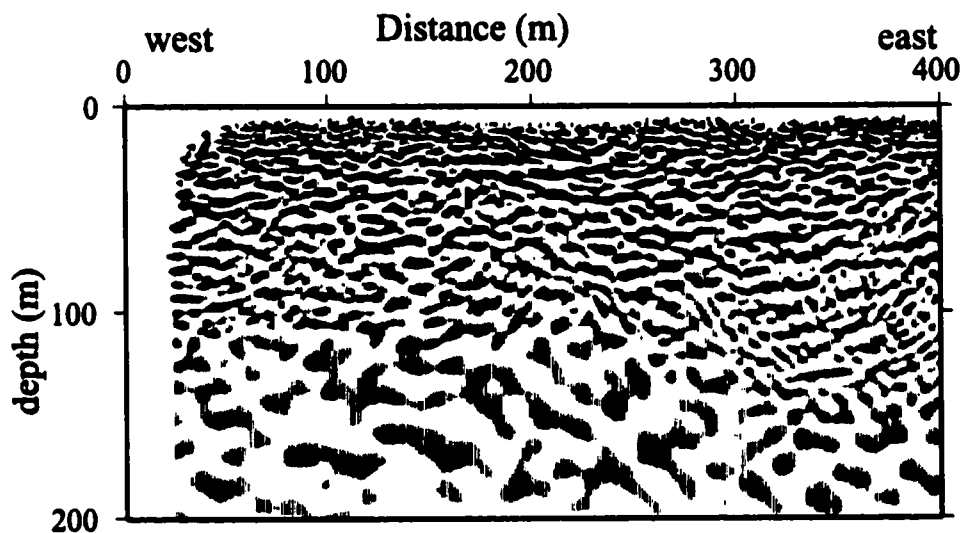


Figure 20 - Depth migrated CMP stack of Bench Line sledgehammer source data. The velocity model (Figure 23) used for the migration was derived from first break analysis. The seismic character of the section is distorted below 100 m from the strong change in the velocity model caused by the large velocity increase from the sedimentary units to the crystalline rock below (Figure 24).

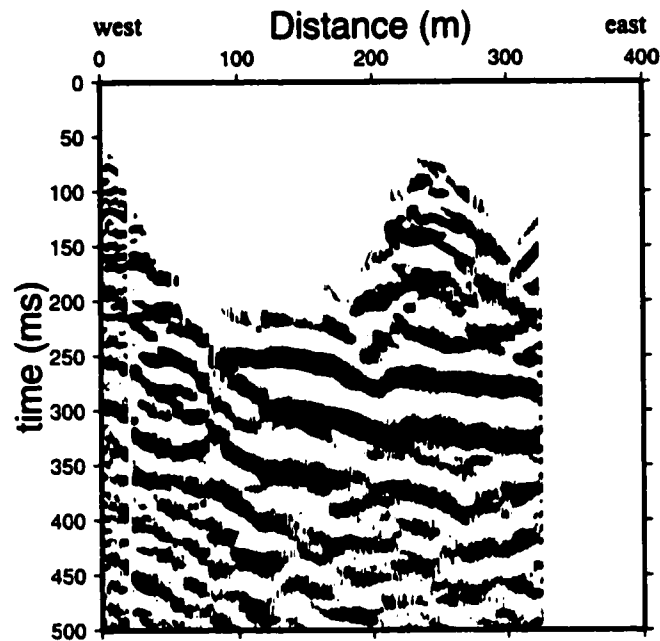


Figure 21 - CMP stack of Bench Line dynamite source data. The gap in the shallow portion of the section is caused by variable source receiver offset in the acquisition geometry. The dynamite data covers only 330 m of the 400 m length profile.

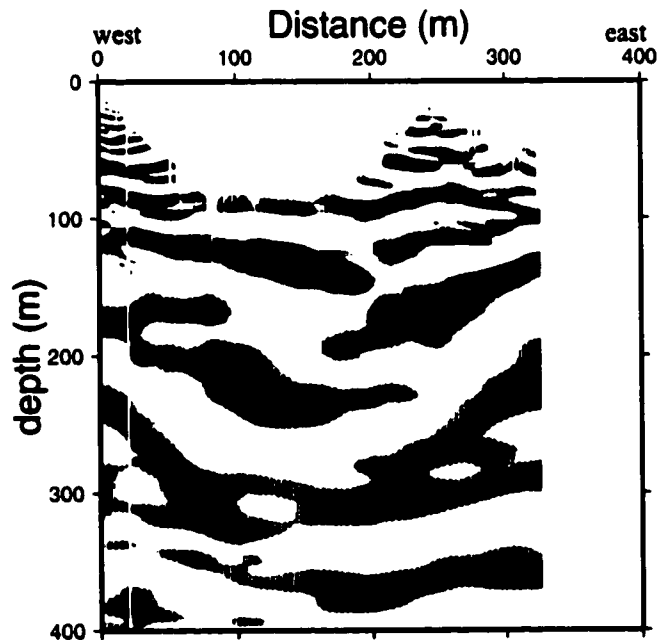


Figure 22 - Depth migrated CMP stack of Bench Line dynamite source data. The velocity model used for the migration is shown as Figure 24. The strong velocity gradient in the model shows in the image as the transition to lower frequency events.

was used to constrain a velocity model that fits the travel times. The initial model of a flat three-layered model representing the stockpile, conglomerate and basement rocks provided a start point for the code. Repeated iterations constrained both the velocities within the layers and the depth of the interfaces between them. Gradually, the shallow velocities and layer thickness were fit to the data and held fixed. The code was iterated to determine velocities and layer thickness of the next layer, allowing only the parameters of the two lower layers to vary until a reasonable fit of the second layer resulted. Repetition of the process continued through the deepest layer. Perturbing individual parameters within the model and observing the related effect on the overall model provided a verification and quality check of the model. Additionally, repetition of the entire process several times with different layer thickness produced similar models each time. Initially, all first break picks were used; however, the chi-square, or goodness of fit did not converge reasonably with repeated iterations. Upon close inspection, first break picks on nine of the 179 shots appeared to be bad, with very high chi-square values indicating the picks did not fit the developing velocity model. Removing these shots from the travel time data set allowed me to quickly improve the chi-square fit of the model. The final velocity model utilized 170 of the shots with a picking accuracy of ± 5 ms and has a normalized chi-square of one (Figure 23). The nine outliers were from the dynamite data set. The picking error of these shots is most likely from the large source-receiver offset, making it possible to miss the first break refraction and pick an adjacent reflection event instead. The picking accuracy (5 ms) used in the analysis was based on the low frequency of the dynamite data. The final model was the starting model for the depth migration velocity model.

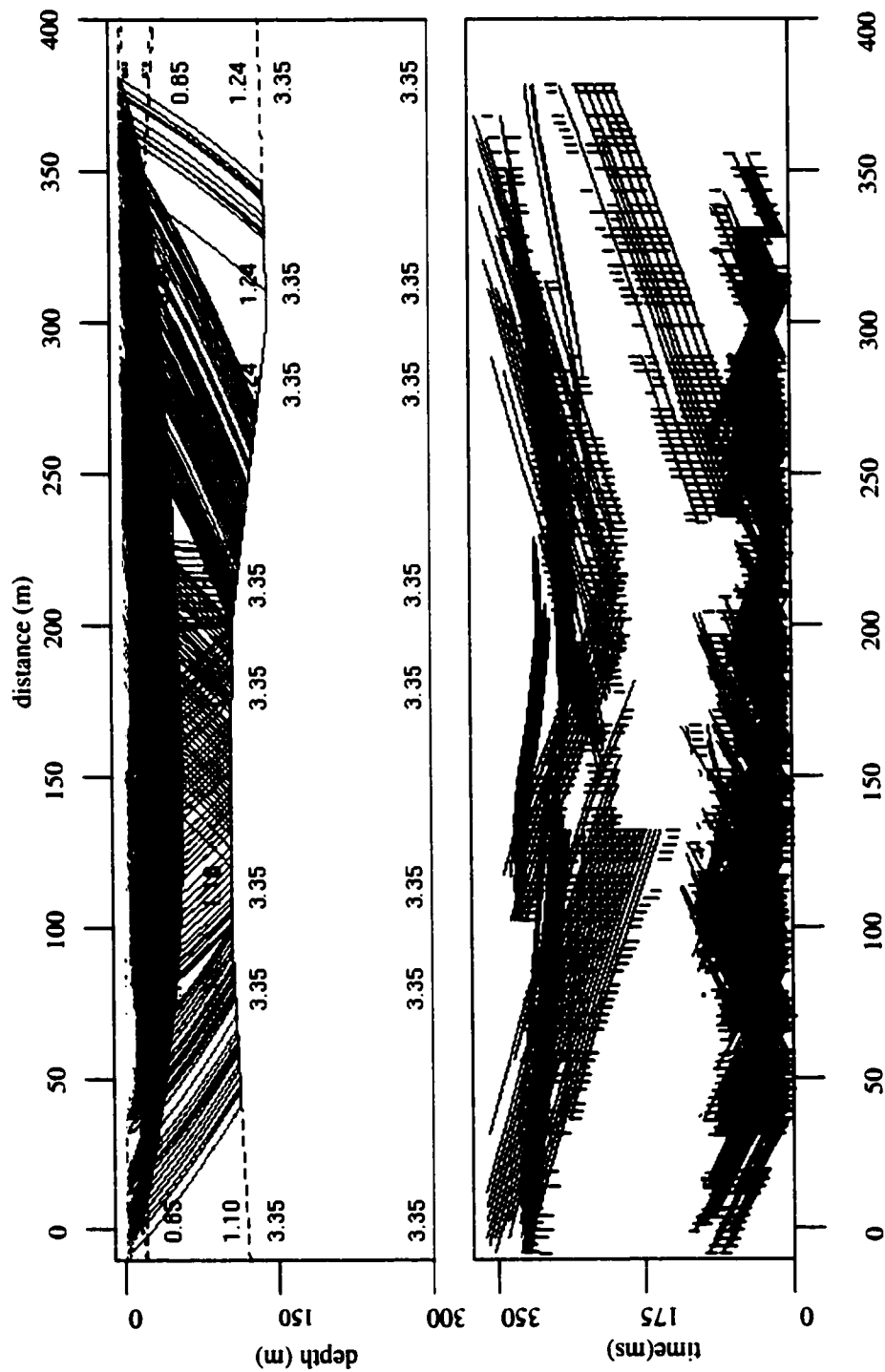


Figure 23 - Final velocity model from first break analysis for the Bench Line. The upper figure shows the resulting velocity model with modeled raypaths. The velocity at the nodes is given in km/s. The lower figure shows the goodness of fit of the modeled times (diagonal lines) in the upper figure to the first break picks of the data (vertical lines). The picks are ± 5 ms in length based on the low frequency of the dynamite data and the strong environmental noise that dominates the sledgehammer data set.

Kirchhoff post-stack depth migration of both source types used a smoothed version of the model (Figure 20, and 22). The smoothed velocity model is shown in Figure 24. Before migration, the CMP stacks were padded on both ends to reduce edge effects. The padding consisted of replicating the first and last 100 CMPs, reversing the order, and adding to (padding) the ends of the section. After migration, the padding was removed. Figure 25 shows the two migrated seismic sections overlain into a single image showing the entire depth of the mine wall.

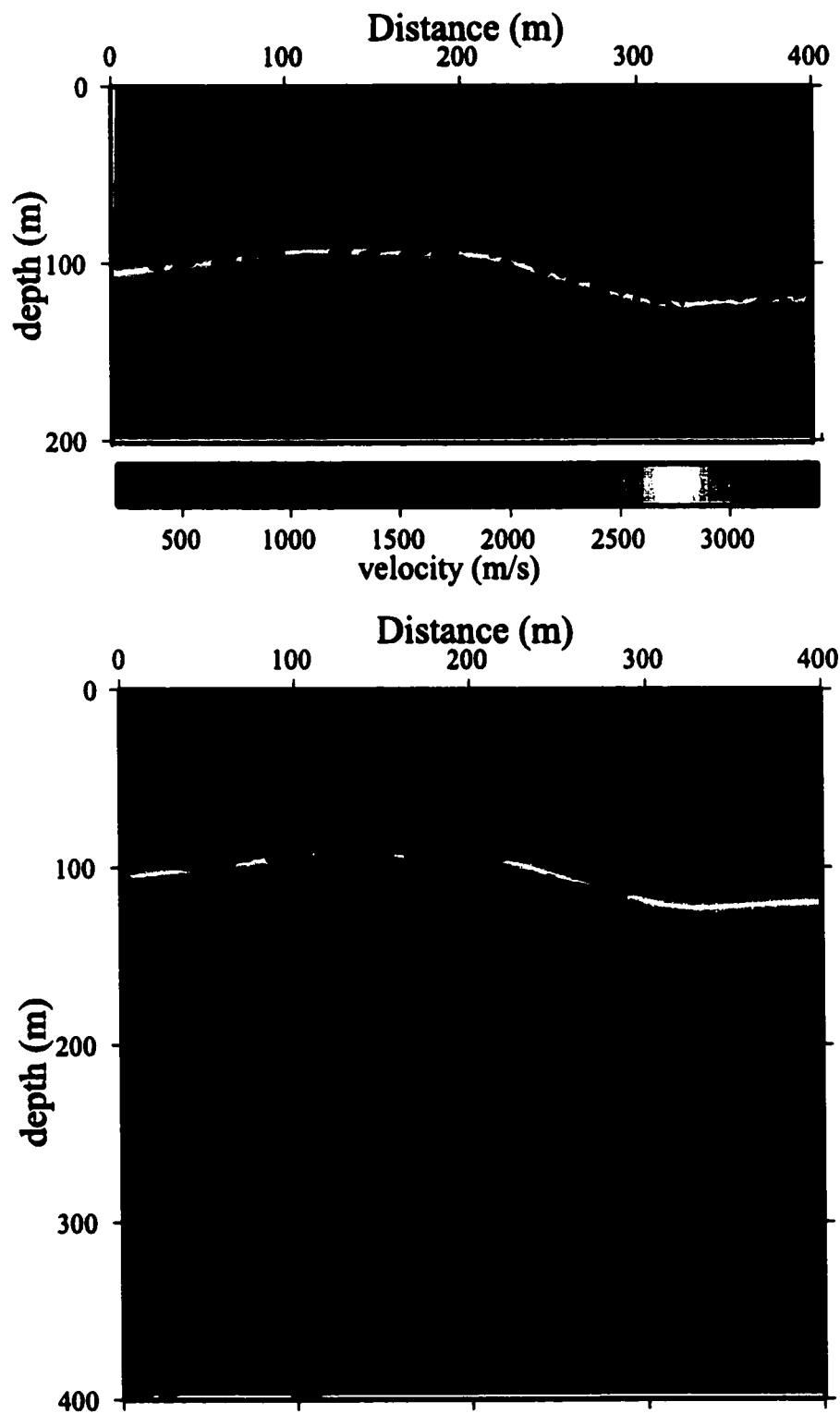


Figure 24 - The velocity model used for the depth migration with depth migrated sledgehammer data (top) and dynamite data (bottom). The model is based on results from travel-time inversion (Figure 23) which were smoothed for migration. The strong velocity gradient at 100 m corresponds to the contact between sedimentary and crystalline units

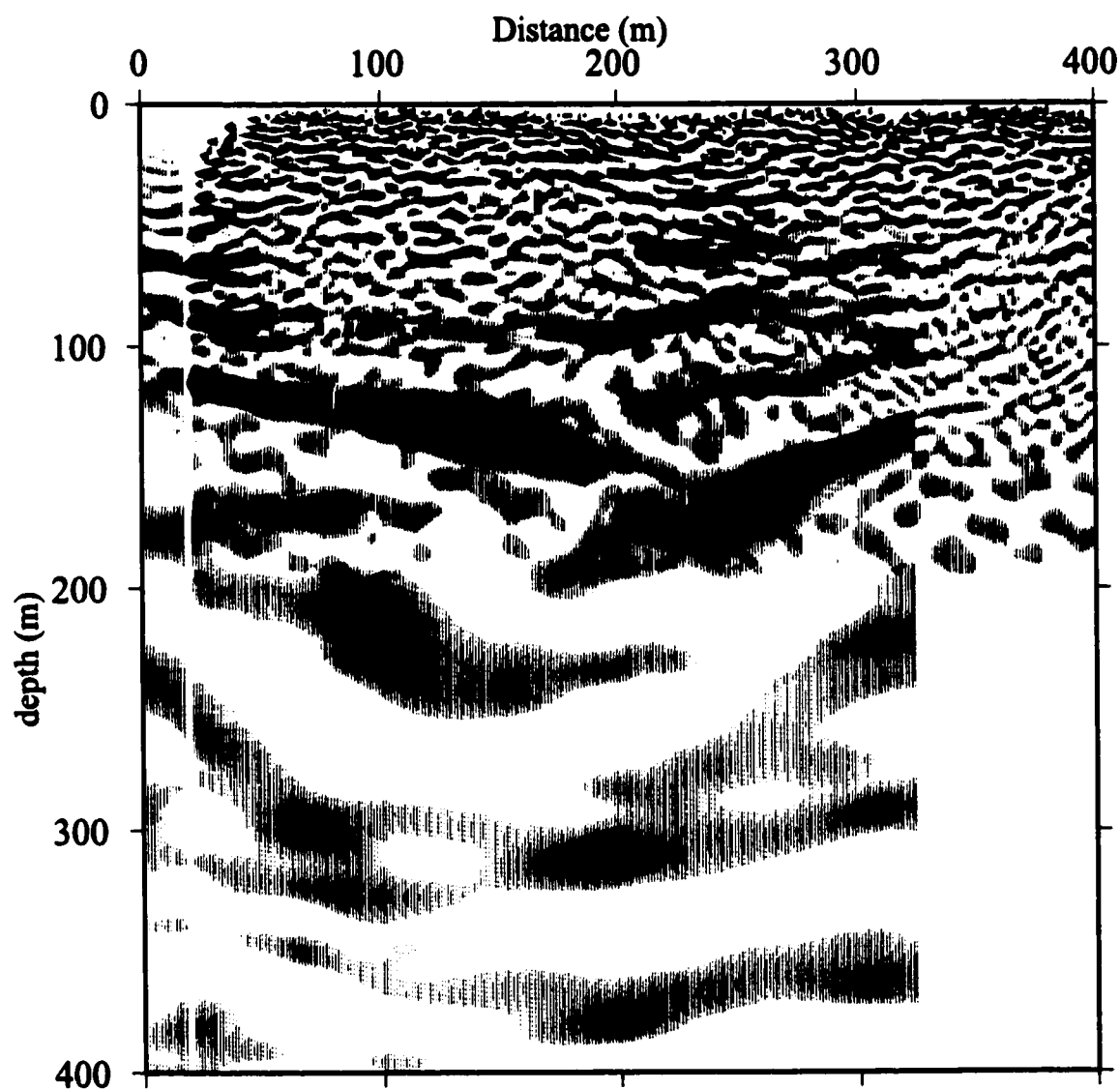


Figure 25 - Combined Bench Line depth migrated section. The sledgehammer data from Figure 20 is in black with the dynamite data from Figure 22 underlain in blue. Although processed separately, the general trends of the two data sets correlate with each other.

Sledgehammer Data

Trace editing / Trace DC removal
 Elevation statics
 Trace equalization
 Bandpass filter (Butterworth 50-183 with slopes of -18 and -36 Db/Octave,
 Notch at 120 Hz)
 Trace mixing (331 and 271 m/s)
 τ -p transform (± 1000 ms/km) / Inverse τ -p transform
 Surface consistent deconvolution (15/60 ms pred. dist./op. length)
 Bandpass filter (30-50-183-240)
 Top mute (remove artifacts from τ -p)
 Bandpass filter (Butterworth 50-183 with slopes of -18 and -36 Db/Octave)
 (remove high frequencies from SCD application)
 NMO applied / CMP Stack
 Kirchhoff Depth Migration (velocity from travel time analysis)

Dynamite Data

Trace editing
 Elevation statics
 Trace DC removal
 Hand Statics (timing correction shots 6-26)
 Bandpass filter (Butterworth 20-140, with slopes of -18 and -36 Db/Octave,
 120 Hz notch)
 Top Mute
 Trace mixing (345 m/s)
 τ -p transform (± 1000 ms/km) / Inverse τ -p transform
 Bandpass filter (0-0-110-140)
 Surface consistent deconvolution (25/150ms pred. dist./op. length)
 Top mute (remove artifacts from τ -p)
 Bandpass filter (Butterworth 20-140, with slopes of -18 and -36 Db/Octave)
 NMO applied / CMP Stack
 Kirchhoff Depth Migration (velocity from travel time analysis)

Table 3 - Processing flow for the Bench Line (sledgehammer/dynamite)

The Concentrator Line

The Concentrator Line is located across the northern entrance to the mine, over a body of massive sulfides at depth (Figure 26). The 300 meter line crossed the entire width of the terrace along the road into the mine. Although data collection included dynamite and shotgun sources, the shotgun data did not penetrate deep enough to image the sulfide body. This discussion deals only with the dynamite source data for the line. Figure 27 is a stacking chart of the dynamite source data of the line. This line had the least amount of environmental noise, making it less complicated to process.

Figures 28 and 29 are plots of amplitude spectra for two shot gathers from the profile. The bandwidth (10-50 Hz) is very similar, but slightly narrower and lower frequency than the amplitude spectra of the dynamite data collected along the Bench Line.

Environmental noise was removed using a bandpass filter with a bandpass of 10 to 80 Hz and a notch filter at 60 Hz to remove AC electrical noise from the nearby mine operations. Use of air blast attenuation reduced high amplitude sound in the gathers. Next, applying minimum phase deconvolution removed ringiness in the data from the notch filter. Trace equalization followed to balance amplitude variations between shots. Figure 30 shows a source gather before and after processing. The processing reduced the low velocity noise in the gathers, but did not remove all of it.

Velocity analysis of the data set started with construction of an initial velocity model based on constant velocity stacks (CVS), then used semblance analysis and stacking

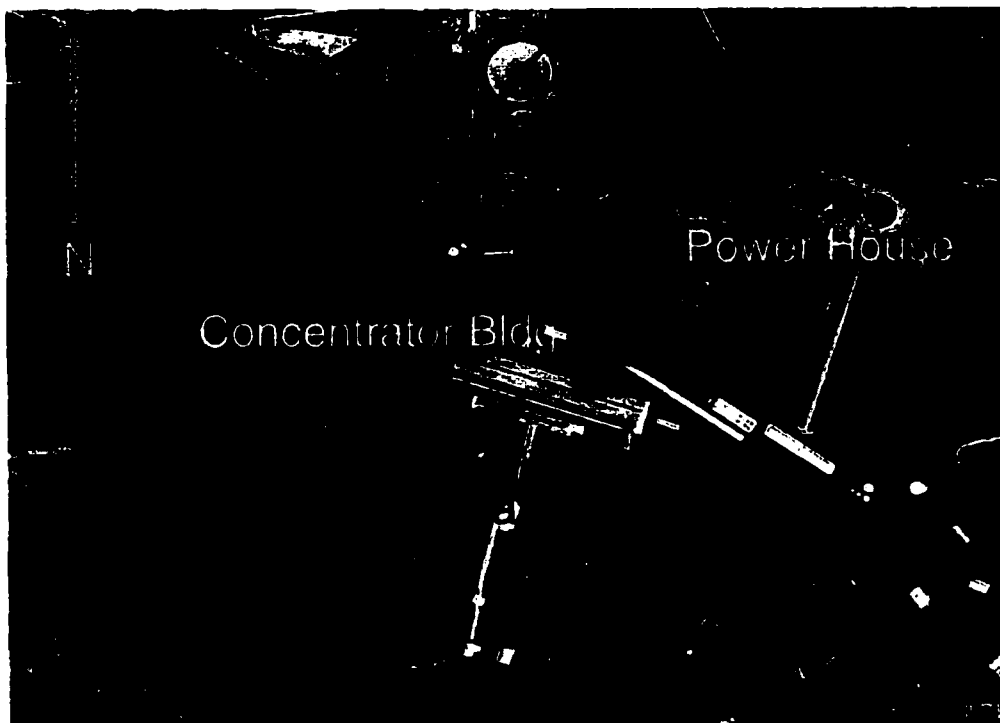


Figure 26 - The Concentrator Line, 300 meters long, is named in reference to the adjacent buildings (USGS, 9/26/1996). The line is situated on the edge of a terrace which serves as part of the main entry into the pit. The northern edge of the main pit is labeled. Both the Concentrator building and the Power House are sources of environmental noise.

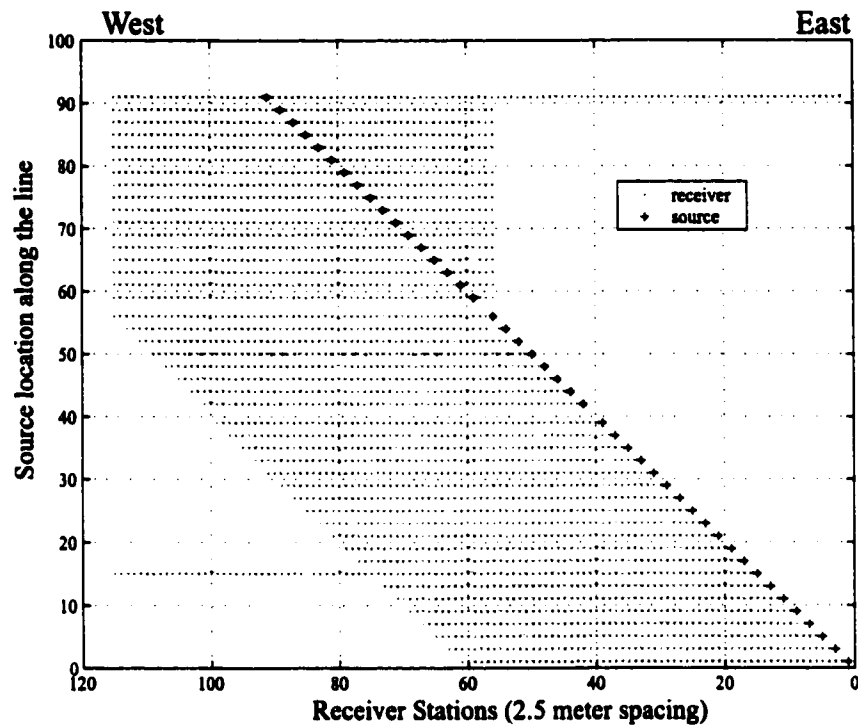


Figure 27 - Stacking Chart for the Concentrator Line dynamite source data. The receiver station interval is 2.5 m and the source interval is 5 m. The 300 meter line has limited offset, as compared to the Gila and Bench Lines, of 75 to 150 meters.

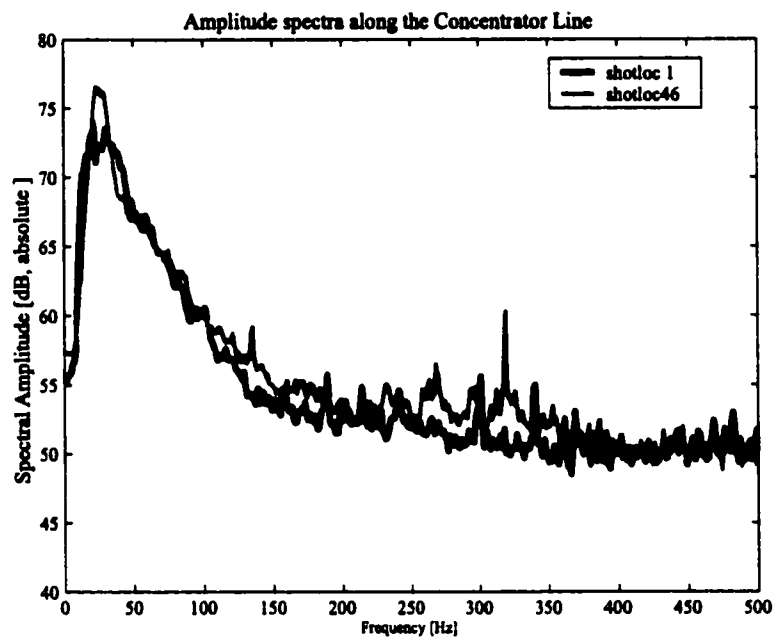


Figure 28 - Absolute amplitude spectra for two dynamite source gathers along the Concentrator Line. Note the low frequency and limited bandwidth of the signal.

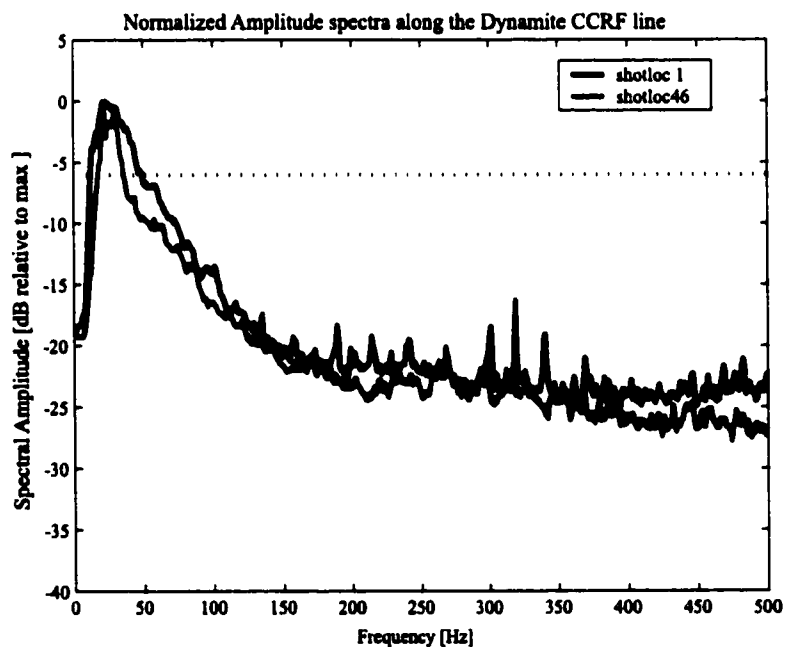


Figure 29 - Normalized amplitude spectra for two dynamite source gathers along the Concentrator Line.

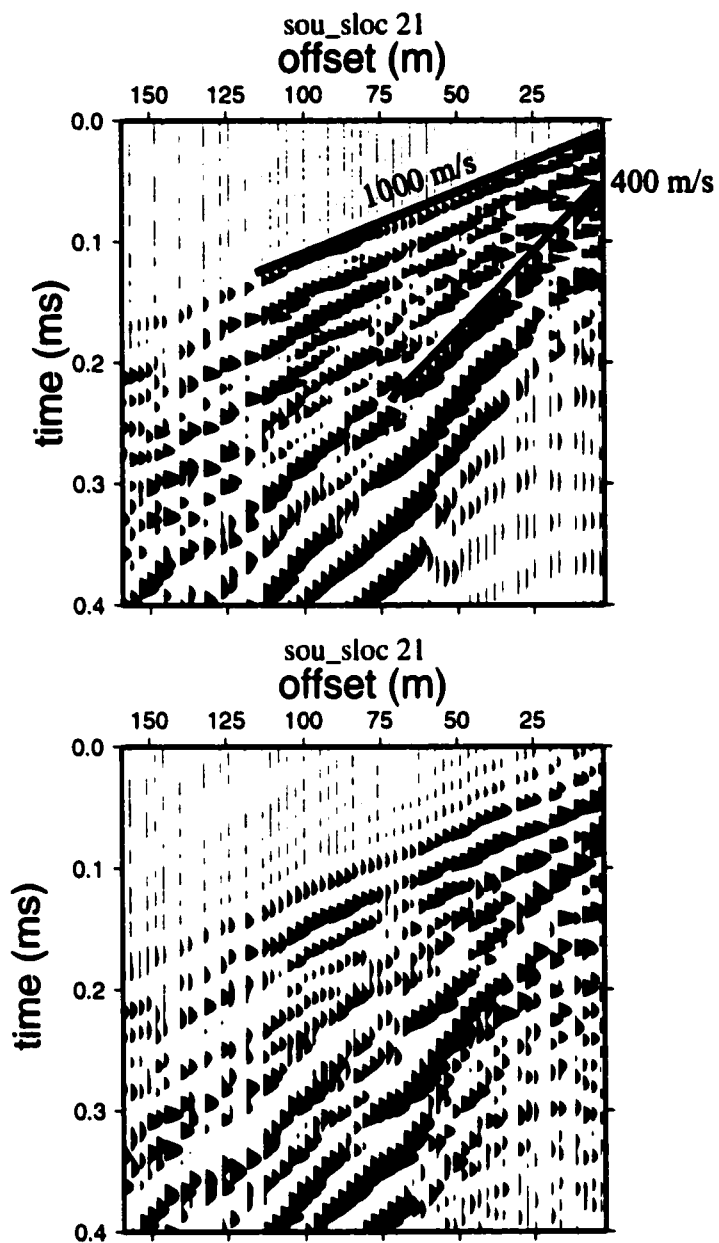


Figure 30 - A Concentrator Line shot gather before (upper) and after processing (lower). The ground roll is reduced by data processing, but not completely removed from the gather.

velocity analysis to develop the final stacking velocity model. Figure 31 shows the resulting CMP stack. The CMP stack contains low velocity linear noise throughout the section. To remove the noise, an F-k fan filter applied to the entire stack removed linear events with velocities between ± 150 m/s. The filtered stack is cleaner, with improved reflection clarity and continuity (Figure 32).

The Concentrator Line did not have long source-receiver offsets necessary for first break travel time analysis. Only two of the 47 shots had large offset ranges. For this reason, the stacking velocity model used for the CMP stack was smoothed for use as a velocity model for time migration and then depth converted for use as a velocity model for depth migration. Prior to migration, the CMP stack was padded on both ends to reduce edge effects. The first and last 100 CMPs were replicated, reversed in order, and added to the ends of the section. After migration, the padding was removed. Figure 33 shows the time migrated image alone and overlain on the velocity model. Figure 34 shows the depth migrated image and Figure 35 overlays the image on the depth converted model. Table 4 summarizes the processing flow for the Concentrator Line, dynamite source data.

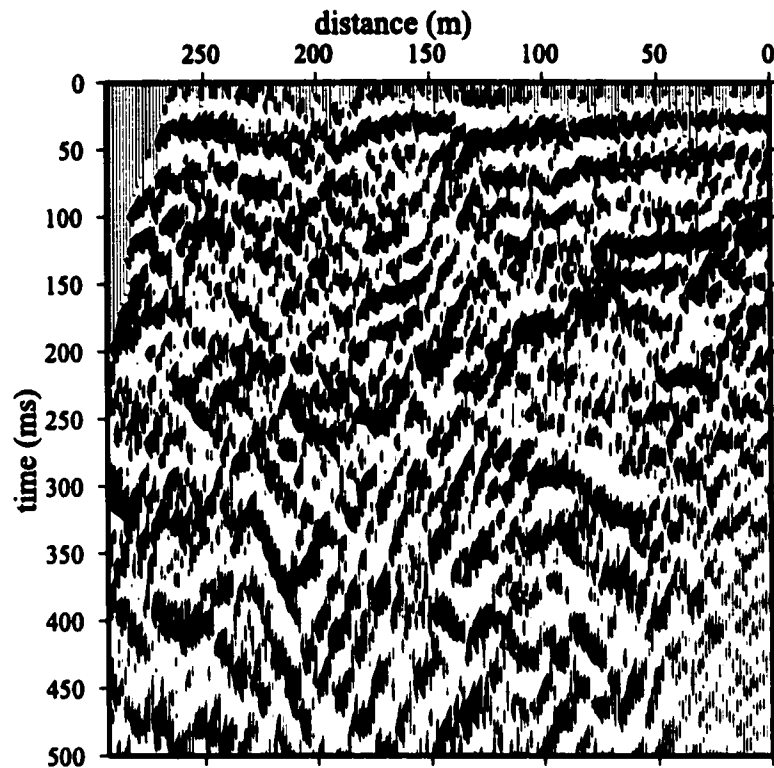


Figure 31 - Initial dynamite source Concentrator Line CMP stack.

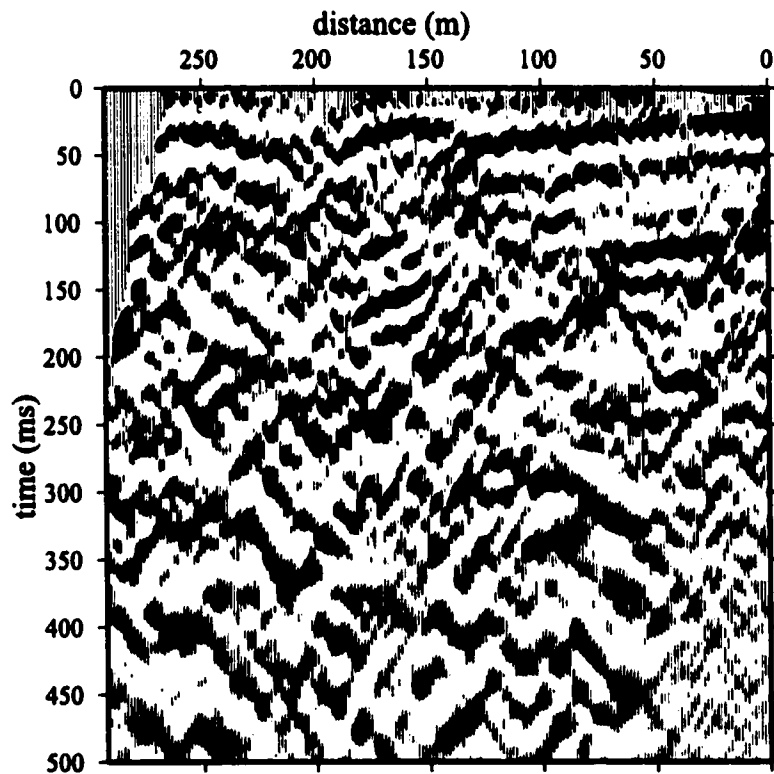


Figure 32 - Initial dynamite source Concentrator Line CMP stack with an F-k filter and minimum phase deconvolution applied to the stack. The F-k filter reduces the low velocity linear events in the section

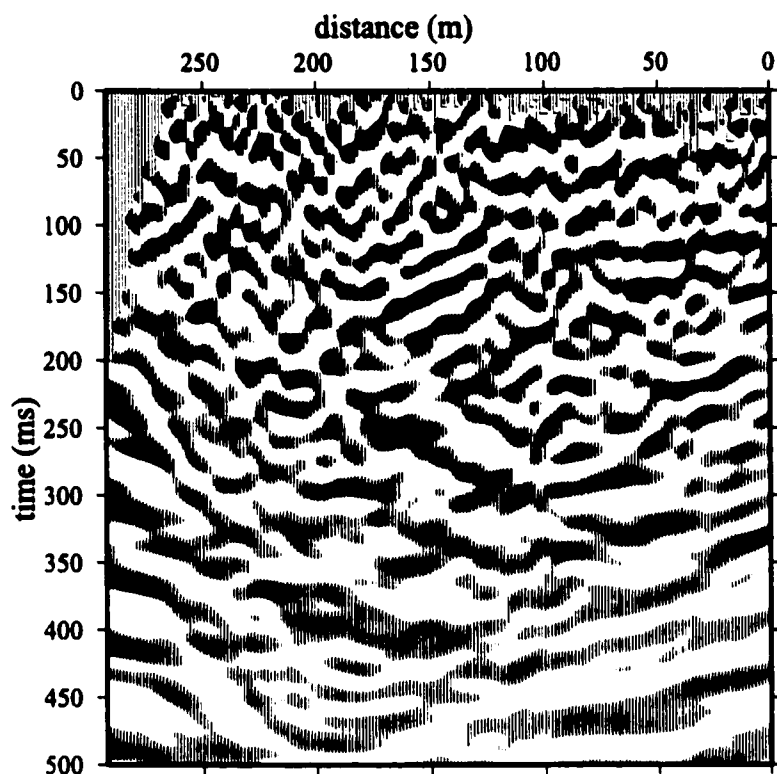
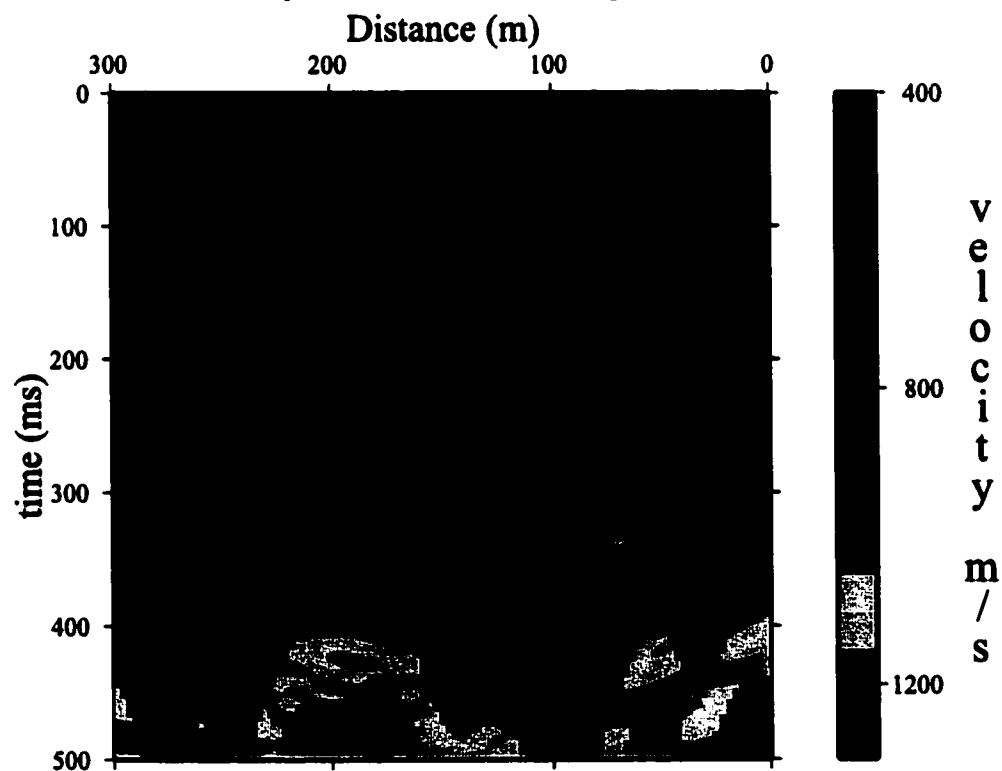


Figure 33 - Time migrated Concentrator Line dynamite source stack (top) and with the velocity model based on stacking velocities (below)



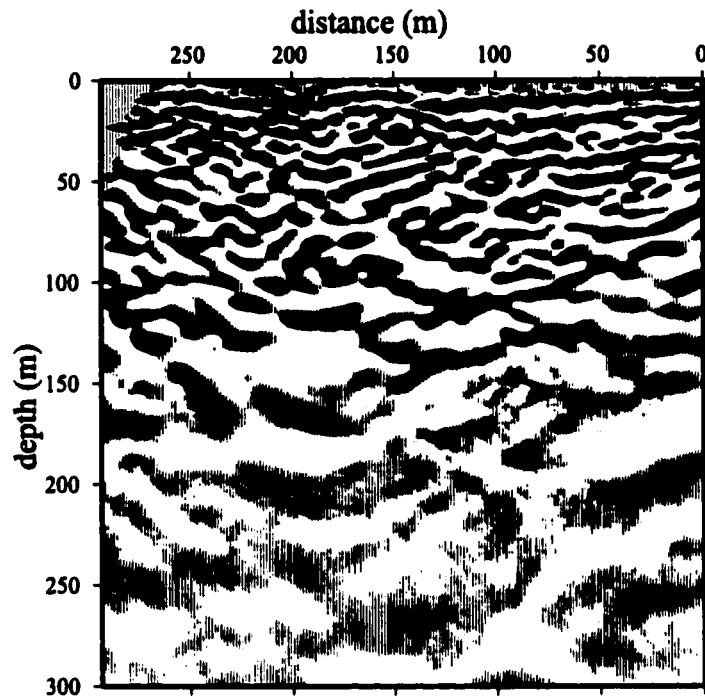


Figure 34 - Depth migrated Concentrator Line dynamite source section.

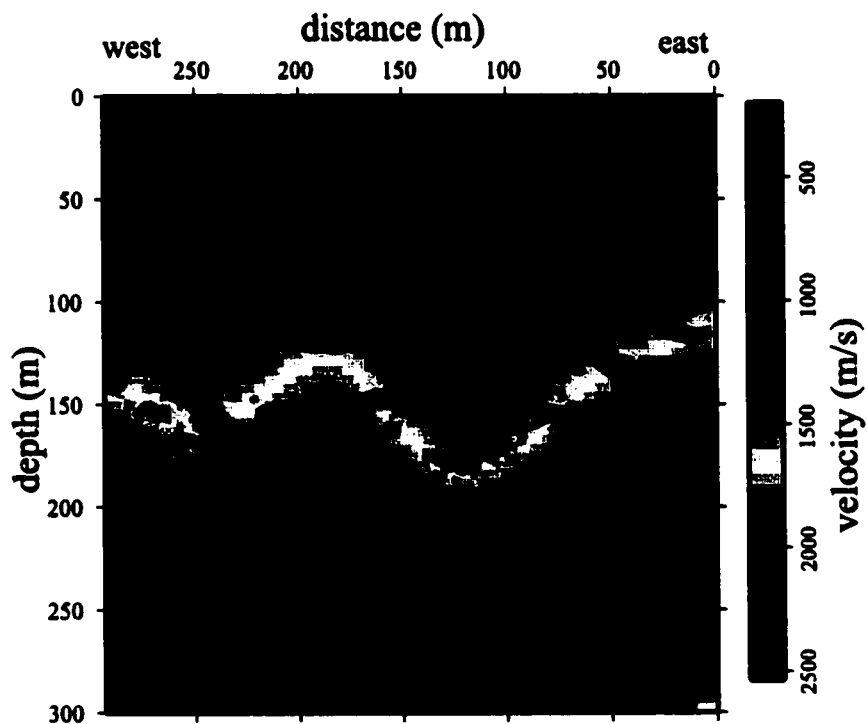


Figure 35 - Depth Migrated CMP stack (Figure 34) of the Concentrator Line dynamite data overlain on the velocity field. The Concentrator Line acquisition was not able to record sufficient far offset data to construct a velocity model from traveltime analysis as was performed for the Bench and Gila Lines. The velocity field was developed by depth converting the stacking velocities used to construct the CMP stack and then smoothing prior to migration.

Trace editing
Elevation statics
Hand Statics (timing correction for shots 4-12)
Trace DC removal
Bandpass filter (0-10-80-120, with notch at 60 Hz)
Air Blast Attenuation
Minimum phase predictive deconvolution (60/15 – op length/pred. dist)
Bandpass filter (0-12-48-60)
Trace Equalization
Velocity Analysis
NMO
CMP stack
F-k filter applied to stack (± 250 m/s)
Kirchhoff Post-Stack Time Migration (smoothed stacking velocities)
Kirchhoff Post-Stack Depth Migration (smoothed and converted stacking velocities)

Table 4 – Processing flow for the Concentrator Line

INTERPRETATION

The Gila Line

Figure 36 shows the depth migrated image of the Gila Line with interpretation.

Sledgehammer data, in blue, covers the upper 150 m of the 300 m deep mine wall. It defines the Mangas conglomerate within the first 100 m of the seismic image as near-horizontal downlapping events above the coarser seismic signature of the crystalline basement rock. The unconformity between the conglomerate and the underlying basement rock is the termination of the downlap against the basement rock. The leach cap appears as a transitional zone between the fine bedding of the conglomerate, and the deeper, slightly coarser signature of the low-grade sulfide.

Geologic information from boreholes near the Gila Line is included in the figure for comparison with the seismic results. Logged depths to the base of the conglomerate and the leach cap are marked with red squares (unconformity). Green diamonds mark the base of the leach cap. The five wells used are all less than 30 meters from the seismic profile, close enough that any change in thickness of rock units is within the resolution of the data. Good correlation exists between the interpretation and the borehole data. The dynamite portion of the data set (Akerberg, 1999), underlying the hammer, in black, is included to show the correlation between the two independently processed source types. A linear feature dipping to the northeast at the right (southwest) edge of the section from 80 m to 200 m is visible on both the sledgehammer and dynamite seismic sections. The limited offset along the feature suggests it may be a fracture in the rock.

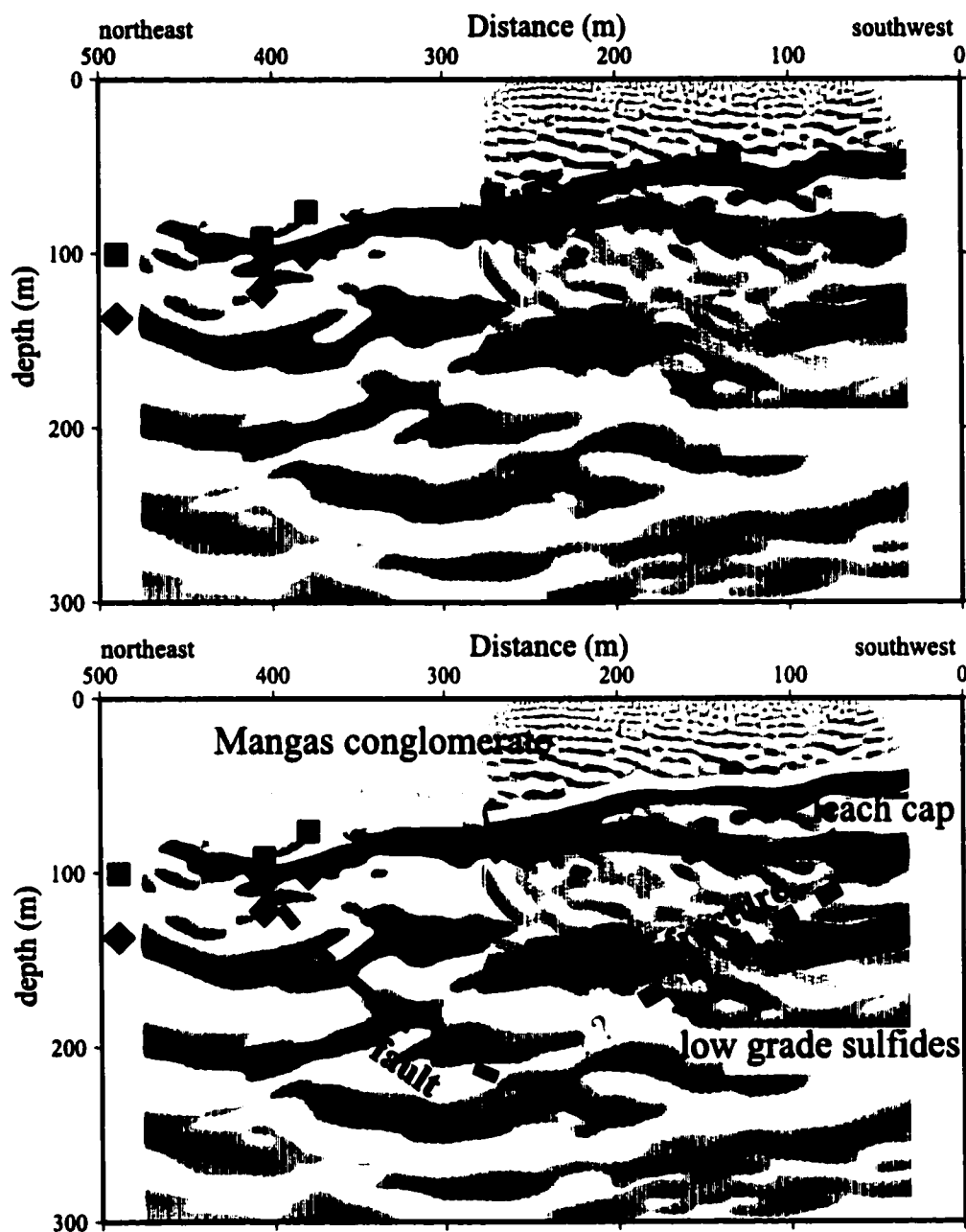


Figure 36 - Depth migrated image of the Gila Line showing the sledgehammer data in blue overlain on the dynamite data (black)(Akerberg, 1999). The migrated image with borehole data only is shown at the top and the interpreted image is below. The colored symbols are from four boreholes in the vicinity of the line. The red squares give the depth to the base of the conglomerate. The green diamonds indicate the logged depth to the base of the leach cap. The interpreted unconformity between the conglomerate and the crystalline rock is shown by the yellow line. The base of the leach cap is indicated by the orange line. The dashed red lines indicate a fault and a fracture interpreted in the data and seen on the mine wall (Figure 4).

Comparison of the seismic interpretation (Figure 38) with the photograph of the mine wall at the Gila Line (Figure 37) correlates the linear feature to the edge of the wall, adjacent to less well-consolidated material, supporting the fracture interpretation. The approximate depth to the unconformity and thickness of the leach cap also compare well with the photograph. Overall, the sledgehammer data for this line appears reasonable to a depth of 175 meters on the north end of the sledgehammer profile and 150 m on the south end, imaging sediments and into crystalline rock across its entire length. Using the center frequency of 80 Hz and interval velocities from the velocity model for the Mangas Conglomerate (1500 m/s) and crystalline rock (3000 m/s), the wavelength of the data varies from 19 m to 38 m deeper in the section. Vertical resolution ($\lambda/2$) is 10 meters near the surface and decreases to 19 meters below 100 m depth in the section.

The Bench Line

The near surface geology of the Bench Line differs from the Gila Line in two respects. The surface unit along the Bench Line is a 30 to 60 m thick layer of stockpile (mine tailings). The low velocity stockpile unit was deposited by loads of mine tailings dumped consecutively along the edge of the mine pit by mine trucks. The stockpile was later compacted by mine equipment and does not have coherent bedding planes, with the possible exception of the contacts between adjacent dump truck loads. During the survey, the stockpile layer was a local focus of the mining operation, excavating the layer for mineral extraction. The Mangas conglomerate (40-130 m thick) lies beneath it. The second difference is the quality of the mineral deposit along the Bench Line. Whereas the Gila Line is situated over a zone of very low quality sulfides that does not contain

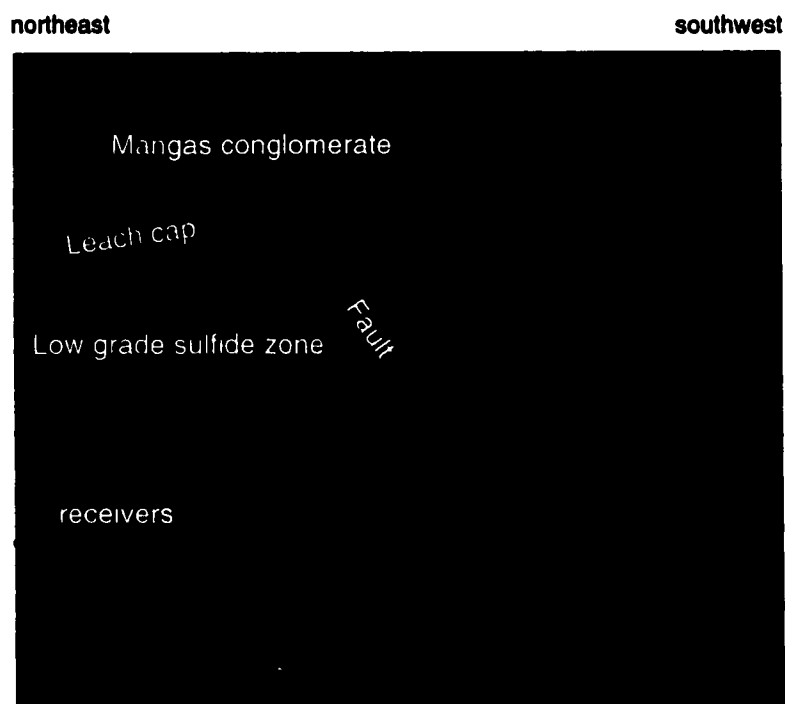


Figure 37 - Photograph of the main pit wall along the extent of the Gila Line. Visible features of the mine wall are labelled.

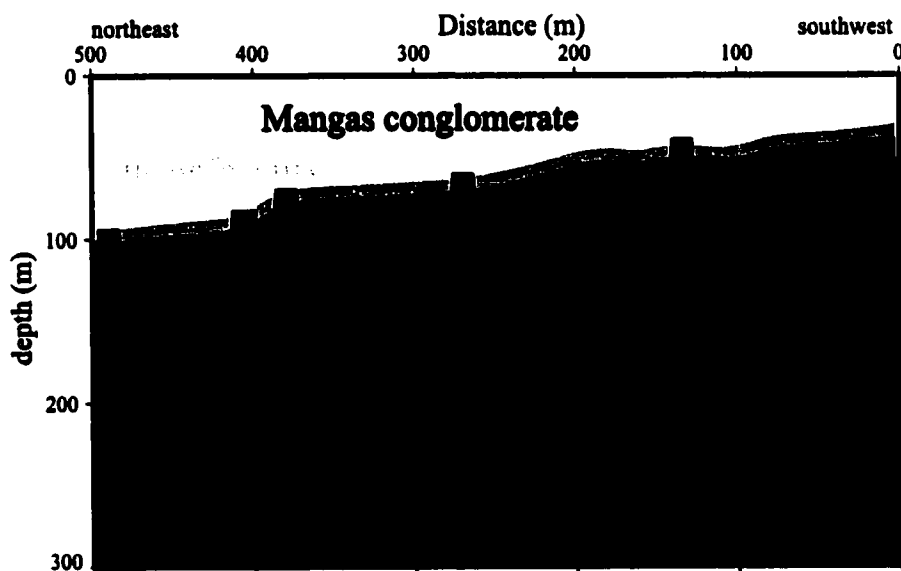


Figure 38 - Interpretation of the depth migrated sledgehammer data from the Gila Line. (Figure 36) for comparison with the photograph above (Figure 37). The mine wall is approximately 300 m deep. The fault seen on the photograph lies beyond the northeast edge of the sledgehammer section. The fracture in the interpretation coincides with the point at which the benches abut the softer sedimentary unit at the southwest edge of the line.

enough copper to be of economic interest to the mining operation, the Bench Line covers high quality chalcocite (one percent) at depth (200 m). Chalcocite, of higher density than the surrounding host rock, has strong seismic impedance, producing strong seismic reflections (Salisbury et al 1996). The presence of chalcocite on the Bench Line should produce observable reflections within the crystalline bedrock, whereas the Gila dynamite data did not. Using the acoustic impedance equation for reflection coefficients, $(\alpha_2 \rho_2 - \alpha_1 \rho_1) / (\alpha_2 \rho_2 + \alpha_1 \rho_1)$ where α represents the velocity of two layers and ρ the density, an estimate of the reflection coefficient of the ore bearing rock can be made. Given a constant velocity of 3000 m/s for the crystalline basement taken from the travel time analysis, calculation of a reflection coefficient rests solely on density contrasts. A density of 2.74 gm/cm³ for the crystalline bedrock (porphyry), 5.80 gm/cm³ for chalcocite and 5.0 gm/cm³ for pyrite are values taken from a text (Telford et al., 1990). The calculated reflection coefficient of one percent chalcocite within the porphyry is 0.005, too small to be observed in the seismic data. The chalcocite, however, appears as a coating on pyrite and other sulfides within the mine (DuHamel et al., 1995) and as such, calculation of a reflection coefficient should account for the densities of all sulfides present in the rock. Mineralized zones along the bench line vary from three to ten percent sulfides (DuHamel et al., 1995). Including one percent chalcocite with nine percent pyrite, the reflection coefficient increases to 0.041. This value is equivalent to a reflection coefficient of a typical shallow interface (Telford et al., 1990) visible in a seismic section.

Figure 39 shows the depth migrated seismic section of the Bench Line with interpretation. The sledge hammer source data (blue) is overlain on the dynamite data (black). The sledgehammer data images the shallow, small-scale features of the first 170 m of the section. The dynamite shows the deeper, large-scale features of the lower 300 m of the section.

The sledgehammer portion of the seismic image shows up to 60 m of stockpile covering the Mangas. The seismic character of the stockpile appears layered and finer than that of the Mangas below. The sledgehammer data accurately images the Mangas to 170 m deep in the section. Within the conglomerate, the seismic signature indicates a linear feature at 110 m distance along the line. Defined by breaks, or truncations starting at 70 m depth, the feature dips to the east. This feature, possibly a fracture zone, is marked in red in Figure 39. The center frequency of the sledgehammer data is 90 Hz. Using velocities for the Mangas Conglomerate (1200 m/s) and underlying crystalline rock (3000 m/s), taken from the velocity model, indicate a wavelength varying from 14 m at the surface to 33 m at depth. The vertical resolution of the sledgehammer data decreases from 7 to 15 m ($\lambda/2$) within the section.

The dynamite data shows the contact between the Mangas and the iron oxide layer (a product of supergene enrichment) at the base of the conglomerate. The contact is delineated by the change in seismic signature from high frequency events to low frequency, high amplitude events. The contact between the iron oxide and the underlying leach cap is located using borehole data with the seismic data, as the iron oxide layer is

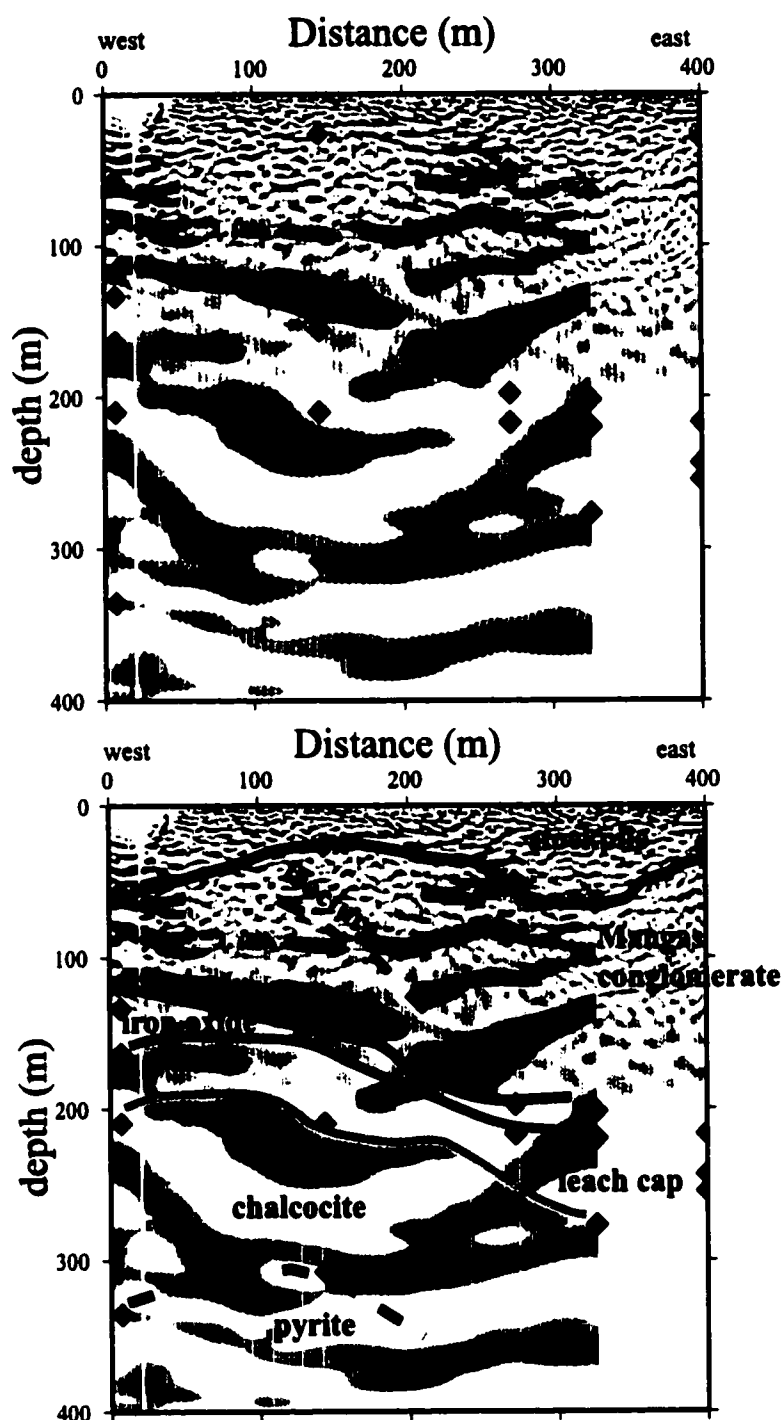


Figure 39 - Depth migrated image of the Bench Line with borehole information overlain (top) and with interpretation (below). The colored symbols locate logged depth to formations from adjacent boreholes for the labeled rock units. The contact between the chalcocite and the pyrite is inferred from borehole data only. The iron oxide zone denotes the weathered contact zone between the conglomerate and the crystalline rock below.

less than 30 m thick. A strong reflector shows at the top of the chalcocite. The reflector implies that the chalcocite is centered within the section at a 200 m depth and does not extend to the east edge of the profile. Locating the pyrite from seismic data alone was not possible. The top of the pyrite is dashed in Figure 39, its placement inferred from borehole data. The dynamite data images the section well from 75 to almost 300 m, 40 meters below the 260 m deep mine pit floor. The linear feature seen in the sledgehammer data also occurs in the dynamite data with its deepest point at 180 m. With a center frequency of 35 Hz and a velocity of 2000-3000 m/s, the dynamite data has a wavelength of 57 to 86 meters. The vertical resolution of the dynamite data is 26 to 43 m ($\lambda/2$) within the section.

The two data sets show good correlation within the effective range of the sledgehammer (up to 170 m deep). The high frequency sledgehammer data agrees with the corresponding low frequency dynamite wavelets within the Mangas, and with the upper and lower contacts of the western portion of the iron oxide. This correlation provides a good data quality check.

Depths to the different units in the section were available from the logs of boreholes drilled near the Bench Line. The depth to the base of each unit is marked as colored diamonds for each borehole used (Figure 39). Each of these boreholes is less 200 ft (61 m) from the profile. Given the 15-20 degree northeast dip of the Mangas Conglomerate, depth to the base of the unit, as indicated by the borehole data, can vary at most by 22 meters from that directly under the profile, easily within the vertical resolution of the data

set. Using the borehole data in combination with the seismic helped to identify the reflections from the leach cap and the chalcocite. Unfortunately, the pyrite sulfide occurs too deep in the section for the seismic to properly image it. Its contact with the chalcocite is based solely on borehole information.

Comparison of the seismic interpretation (Figure 41) with a photograph of the mine wall (Figure 40) confirms the relative thickness of the stockpile layer as approximately 30 m, or two benches in the mine wall (one bench is 15m high). The Mangas is visible over five benches, or 75 m, its thickness increasing to the east. The red contrast of the iron oxide is clearly seen on the east end of the line. Below, the remaining rock units below the unconformity are not distinguishable on the mine wall.

The Concentrator Line

Although located north of the main pit of the mine, the mine operators estimate a high-grade porphyry deposit at depth (289 to 412 m) underlying this area (Steegan, pers. com., 1998). Borehole data is not available for correlation with the seismic data.

Figure 42 shows the interpreted time migrated image and Figure 43 shows the interpreted depth migrated image. Without correlating geologic information on the subsurface environment, interpretation was based on several factors: Knowledge of the local and regional geology, changes in seismic signature within the section, velocity changes in the migration model and similar velocities to those defining the same units in the Gila and Bench Lines. Both images show a surficial unit covering the Mangas Conglomerate.

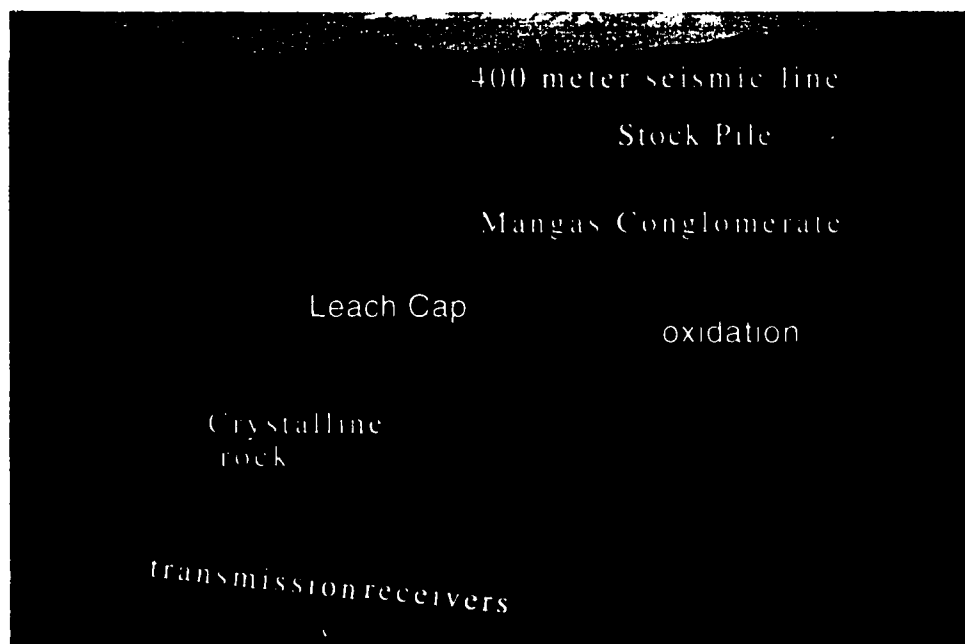


Figure 40 - Photograph of the Bench Line showing the mine wall. Visible units are labelled for comparison with the interpretation made from the depth migrated section below.

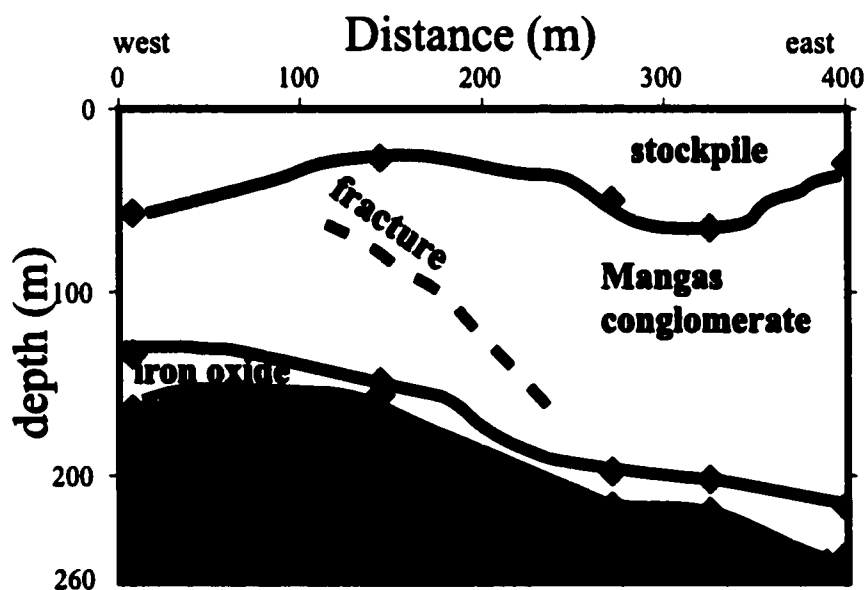


Figure 41 - Interpretation taken from the depth migrated section (Figure 39) for comparison with the mine wall photograph (above). The interpretation is limited to the depth of the mine wall (260 m). The light and dark colors represents the sedimentary sequence and crystalline units respectively.

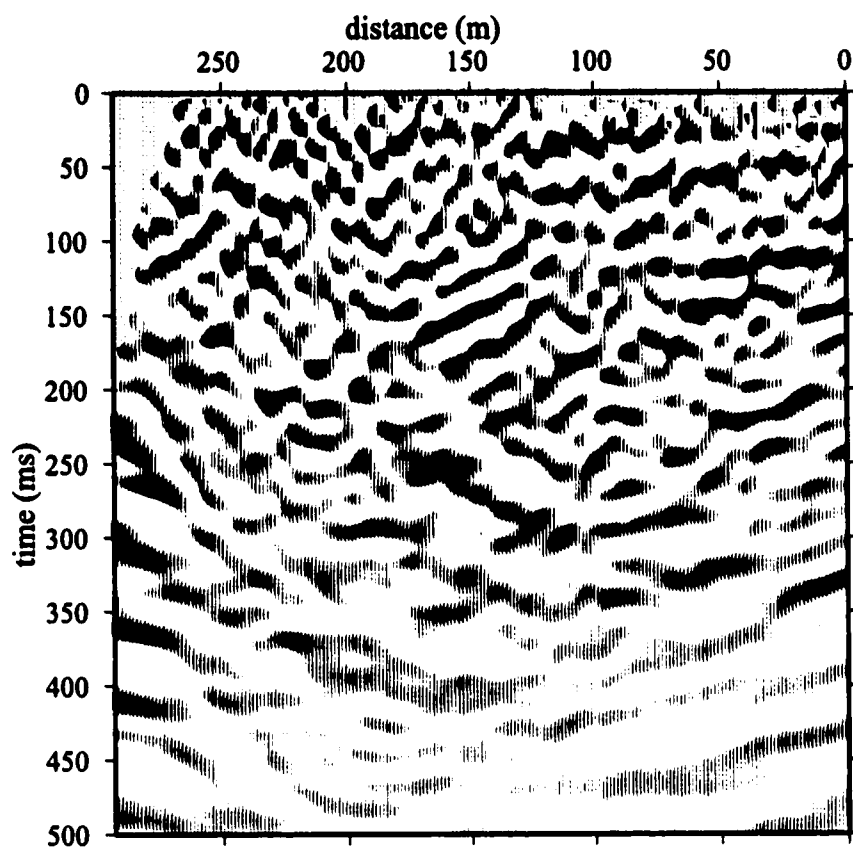
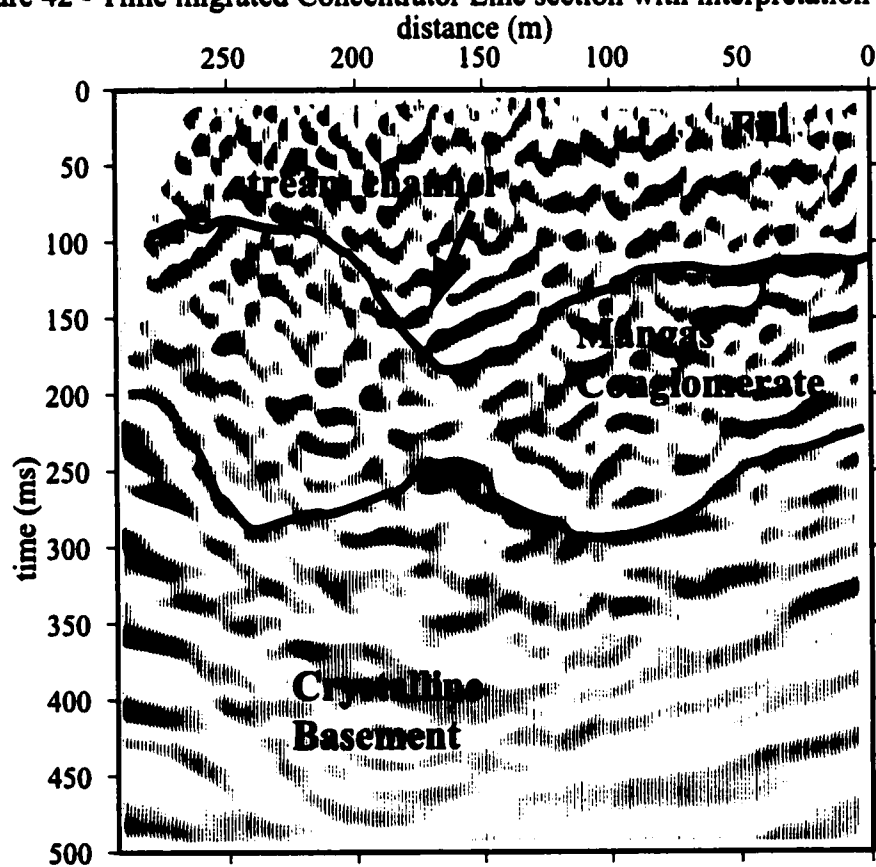


Figure 42 - Time migrated Concentrator Line section with interpretation (below).



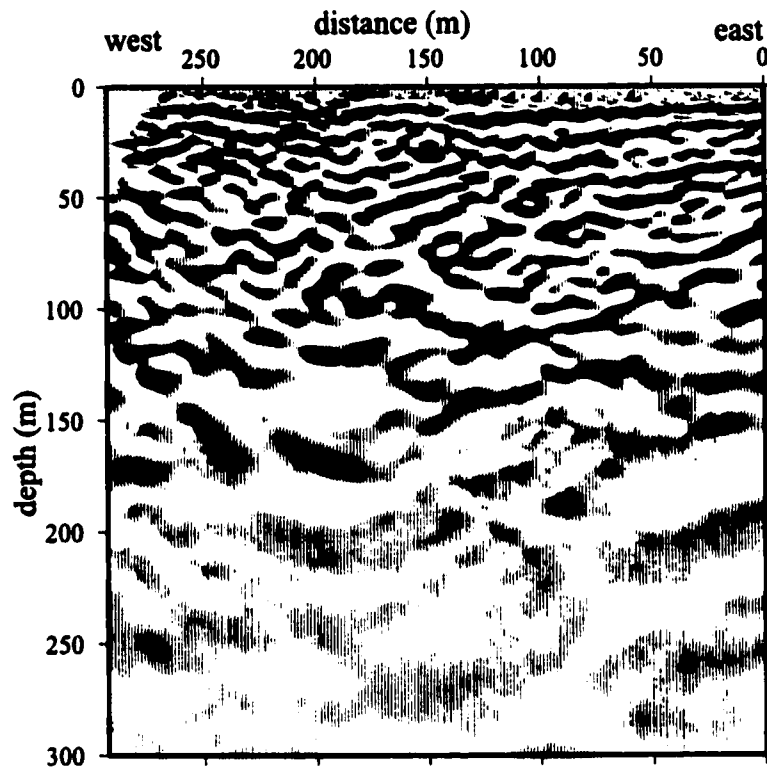


Figure 43 - Depth migrated Concentrator Line dynamite source section with interpretation (below).

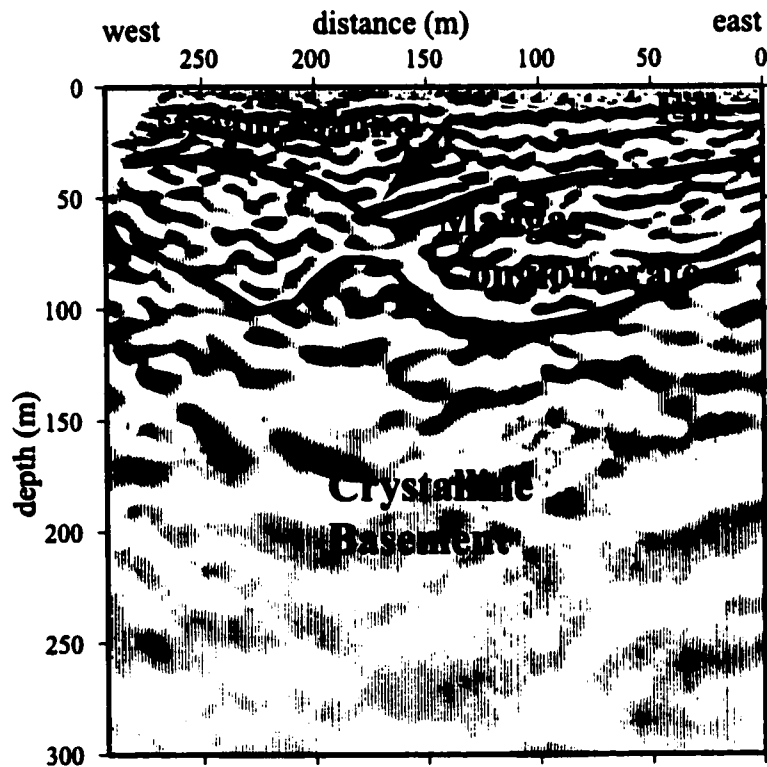


Figure 44, a high-resolution aerial photo, indicates this unit to be fill, developed by the mine operation combined with alluvium, covering the main entrance into the mine.

Maps of the area indicate the seismic profile extends over a 15 m high terrace constructed of this fill. A 75 m wide feature in the upper surface of the Mangas appears to be carved into the conglomerate 90 m from the west end of the line. Close examination of the seismic signature of the unit indicates that it was used to fill in this feature. The signature of the fill appears flat, but the signature of the deeper portion of the unit roughly parallels the contact between it and the conglomerate, implying the top of the Mangas was the main surficial unit prior to mine activity. Given the surface outcrop of the Mangas at the Gila Line, and its exposure at the Bench Line, this is a reasonable conclusion. A feature cut into this erosional surface could be natural or manmade. An excavation of 30 m into the conglomerate could have been an abortive attempt at reaching the deeper ore bearing units, with one side of the depression a steep face and a gentle ramp on the other. More probable, the depression was simply cut by a stream channel running through the area. Surficial features (i.e. streambed, documentation of early mine operations outside the pit) to corroborate either interpretation have since been obliterated by mine operations in the vicinity. The location of the stream channel along the profile is marked in Figure 44.

The Mangas Conglomerate is approximately 75 m thick in the section. Its seismic signature is uniform, but is coarser than that of the roadfill. It lies unconformably over the crystalline basement rock. The unconformity between the conglomerate and the basement rock is clearly seen in the section, varying in depth from 110 to 150 m.

Beneath, the signature of the crystalline rock appears constant and diffuse from 110 m to

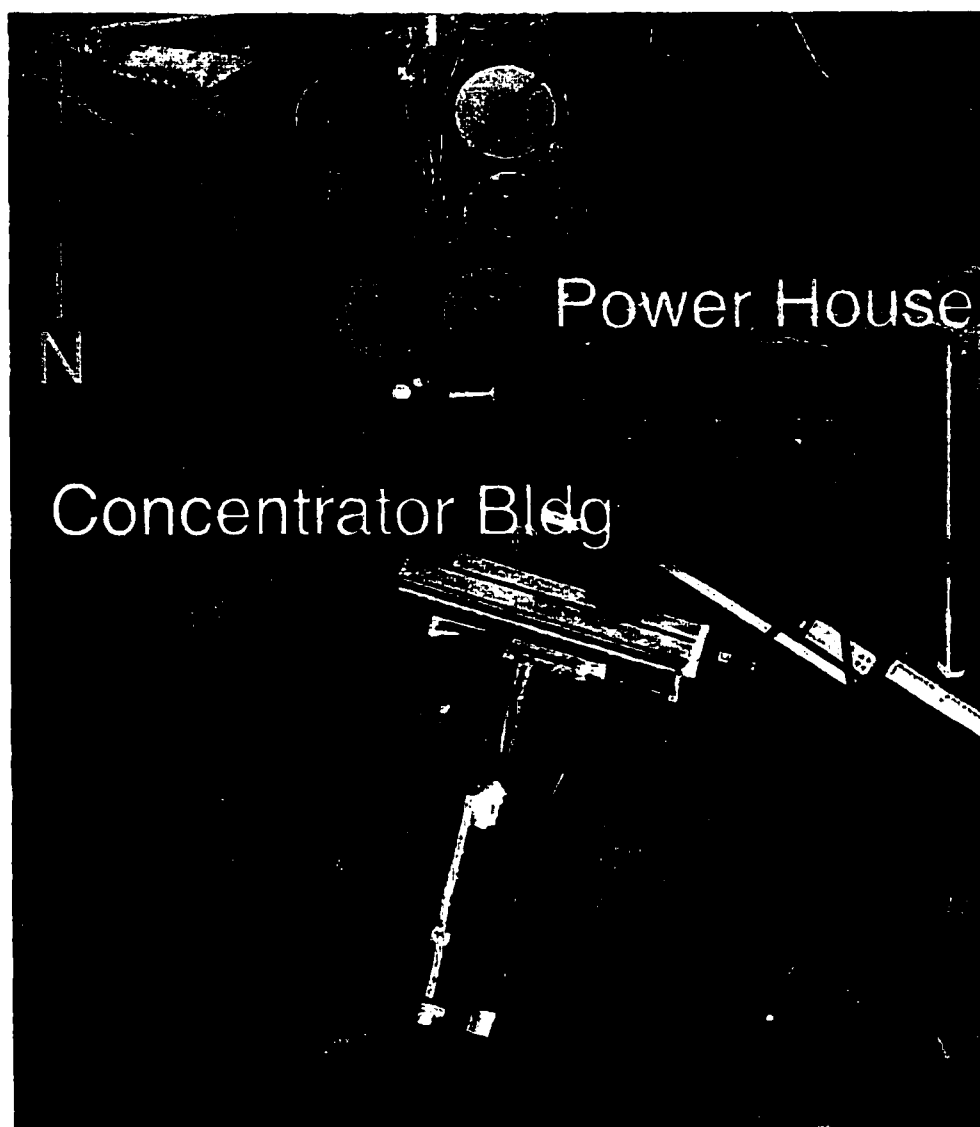


Figure 44 - A close-up view of the Concentrator Line. The 300 m line is located along an access area to the mine along the edge of a 15 m high manmade terrace (labeled). The location of the stream channel, interpreted on the seismic image (Figure 43) is also marked. The mine operation buildings north of the line obscure any surficial indicators that might help to verify the the interpretation (USGS, 9/26/1996).

the base of the section (300 m). The constant signature of the crystalline rock does not show any variation of character as seen by the high-grade deposits on the Bench Line, and expected for this line. During the survey, the mine was in operation, restricting the profile line to an area away from the main traffic into the pit. This limited the accurately imaged depth of the section to less than 300 m, not deep enough to reach the high-grade sulfides below. The center frequency of the dynamite data is 30 Hz and using velocities from the velocity model of 800 to 2500 m/s, wavelength varies from 26 to 83 meters within the crystalline basement. The vertical resolution ($\lambda/2$) varies from 13 m near the surface to 42 m at depth.

DISCUSSION AND CONCLUSIONS

Despite data collection in the midst of an operating mine producing ambient noise from excavation, transportation, and a dense electrical power grid, this study demonstrated the capability of shallow high-resolution seismic reflection techniques to image the complex subsurface environment of a copper mine. Acquisition of data from two separate seismic sources having different frequency bandwidths allowed us to image the entire depth of the mine walls. The hammer data shows shallow, fine scale features and the dynamite data successfully images large-scale deeper features such as fractures, buried erosional features and changes in mineralization.

All three profiles of the survey easily imaged the shallow sedimentary units, even showing bedding. The unconformity between the conglomerate and the crystalline basement rock appeared as a strong event in each of the data sets. The Bench and Gila lines showed the difference in seismic response between areas with and without high-grade copper sulfide deposits. The Bench seismic image has strong reflections below the unconformity that correlate well with borehole data indicating a zone of up to ten percent sulfides containing up to one percent chalcocite (DuHamel et al., 1995). The Gila Line, which overlies an area containing one to two percent sulfides, shows no strong reflectors below the leach cap (Steegan, pers. comm., 1998).

Although a major focus of the survey was its use as a reconnaissance tool for mine operations, ongoing mine operations caused major obstacles in data collection and in the

data itself. The noise from mine equipment, both stationary and mobile, strongly pervades the data sets. The noise required complex filtering techniques to remove it from the gathers without degrading the signal. For the higher frequency and lower amplitude sledgehammer data it was a very serious concern, dominating the gathers. For the lower frequency, but stronger amplitude dynamite data, the noise was present but not dominant. Filtering techniques applied to sledgehammer data were also applied to dynamite data, but the effect on the gathers is less significant. The filters used (F-k and τ -p) allowed me to remove groundroll, and by keeping the entire offset range acquired in the field, image near surface features, such as those within the sedimentary sequence that might otherwise not be visible had an inside mute been applied. At the same time, using different filters aided in data quality control. Processing artifacts and limitations of using only one type of filter do not affect the entire data set. The filters ultimately used for each line were those that most effectively reduced the noise and had the least affect on the data for each line. In the end, the consistency of the differently processed data sets provided a valuable check for the validity of the overall-processing scheme.

The use of photographs of the mine wall along the Bench and Gila Lines for comparison with seismic images was of great benefit. The sedimentary units are visible in the photographs, however, the units below the unconformity are not as distinct due to their igneous and metamorphic textures. Correlations were limited to the stockpile, conglomerate and iron oxide units. The photographs also provided visible confirmation of shallow structures (fracture zones). When used with the borehole data, interpretation

of both the depth and thickness of the different rock units were verified across the section, not limited to discrete points.

For the Concentrator Line, mine activities restricted the placement and length of the seismic profile. The initial 200 m of the seismic section clearly image the overlying sedimentary units and the unconformity below. Although the 300 m length of the profile was not sufficient to reach the depth of the high-grade porphyry, the resulting seismic image shows details of the contact between the surficial units, illuminating an old stream channel. The unconformity below the conglomerate is well imaged, however, the seismic signature below shows little to no variation that could be used to interpret individual units. The use of a converted stacking velocity model for migration of this profile should be considered a contributing factor in the non-distinct nature of the lower portion of the depth migrated image.

Accurately locating of the top of the mineralized zone and fault zones is important for mining. For the Tyrone mine, reconnaissance uses a grid of 1000 feet deep boreholes, placed every 200 feet across the mine area. As of 1998, 4000 boreholes had been drilled at a cost of 25 dollars a foot (Steegan pers. com., 1998), for a total cost of 100 million dollars. Utilization of seismic methods could reduce the number of boreholes needed to characterize the ore body, and reduce costs. This seismic survey cost roughly 60 thousand dollars. A combined seismic-borehole data set would provide continuous coverage of the ore body with the option for detailed investigation of points of interest. Excavation could then be directed to specific areas in the mine. Knowledge of fault

zones or weak zones in the rock, provided by the seismic data, is important for excavation purposes, and for safety of mine personnel operating equipment in the immediate area. Location of near surface structures is also important for identifying those that control local groundwater flow.

The use of seismic techniques will add additional costs to mine operators. As of September 22, the current price of copper is 22 cents per pound on the London Metal Exchange. As of 1999, 160 million pounds of copper have been extracted from the mine (Phelps-Dodge Tyrone: www.phelpsdodge.com/index-pduc.html). With the low return per pound of product, disruption of mine operations to conduct a seismic survey with minimal environmental noise seems unlikely as cessation of mine activity increases mine operational costs. Cost effective seismic reconnaissance within the mine will require signal conditioning to remove noise from operating mine equipment.

Final observations focus on the frequency content of the data. Figure 45 shows normalized spectral amplitudes for each source type along the different seismic profiles. Low frequencies dominate the dynamite data sets for all three lines, suggesting that dynamite may not be a good seismic source for this environment and that a vibroseis source may provide higher frequencies to image deep within the subsurface at a finer resolution. As expected, the sledgehammer data include higher frequencies than the dynamite. The Gila sledgehammer data has a bandwidth of slightly more than two octaves; however, the Bench sledgehammer data bandwidth is three octaves. The only difference between the sledgehammer data sets is the Bench Line located over the low

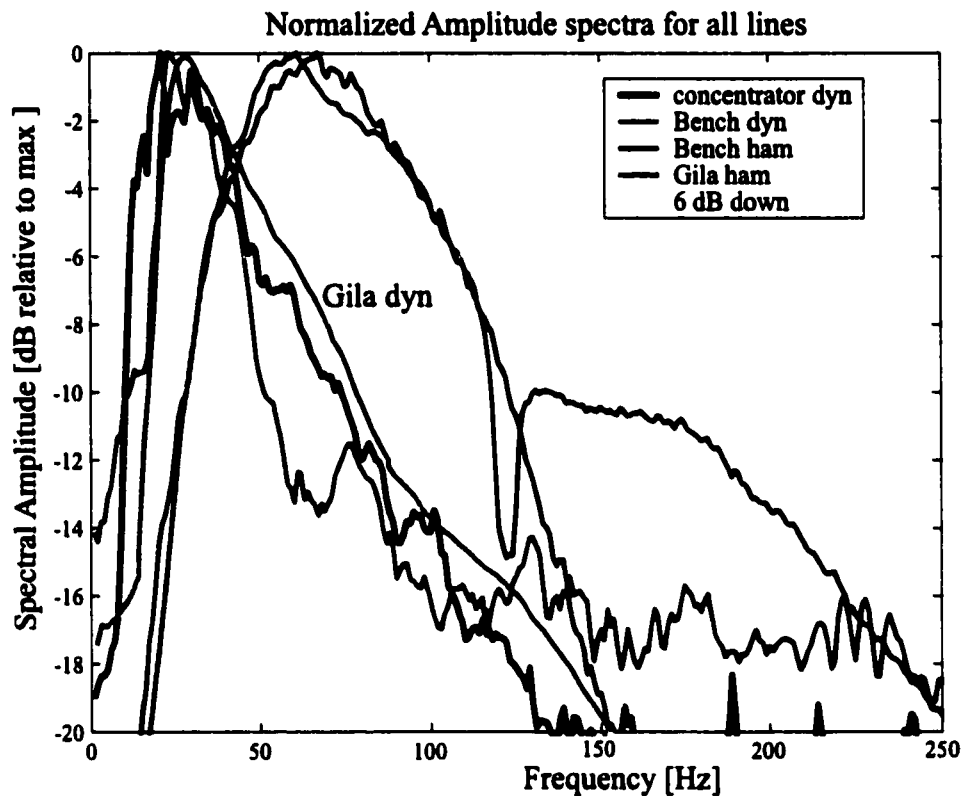


Figure 45 - Normalized amplitude spectra from all lines and source types for the Tyrone study. The light blue line is from Akerberg (1999) for Gila Line dynamite source data. The other spectra are from spectra plots shown in the processing portion of this document. The dynamite spectra from all three lines show low frequency content and are centered around 25 Hz. The Gila sledgehammer data show higher frequencies with the main lobe centered around 70 Hz. The spectra from the Bench Line sledgehammer source data show the same low frequencies as the Gila sledgehammer data, but the bandwidth extends to 180 Hz (a notch filter was applied at 120 hz)

velocity (less than 500 m/s) stockpile unit and the data does not reach the unconformity at the top of the crystalline rock. The Gila Line crosses the Mangas Conglomerate (800 m/s) and includes a reflection from the unconformity. Whether the reduced bandwidth of the Gila sledgehammer data set can be linked to a reflection from a rough crystalline boundary is beyond the scope of this study.

REFERENCES USED

- Adam, E., Milkereit, B., Mareschal, M., Barnes, A., Hubert, C., Salisbury, M., 1992, The application of reflection seismology to the investigation of the geometry of near-surface units and faults in the Blake River Group, Abitibi Belt, Quebec: *Canadian Journal of Earth Sciences*, **29**, 2038-2045.
- Adam, E., Milkereit, B., Mareschal, M., 1998, Seismic reflection and borehole geophysical investigations in the Matagami mining camp: *Canadian Journal of Earth Sciences*, **35**, 686-695.
- Adam, E., Perron, G., Milkereit, B., Wu, J., Calvert, A., Salisbury, M., Verpaelt, P., Dion, D., 2000, A review of high-resolution seismic profiling across the Sudbury, Selbaie, Noranda, and Matagami mining camps: *Canadian Journal of Earth Sciences*, **37**, 503-516.
- Akerberg, Peeter, 1999, Estimation of stochastic parameters from crustal seismic data: Ph.D thesis, Rice University.
- Bates, R.L., Jackson, J.A., Eds., 1987, *Glossary of Geology*, third edition: American Geological Institute.
- Calvert, A.J., Li, Y., 1999, Seismic reflection imaging over a massive sulfide deposit at the Matagami mining camp, Quebec: *Geophysics*, **64**, 24-32.
- Duhamel, J.E., Cook, S.S., Kolessar, J., 1995, Geology of the Tyrone Porphyry Copper Deposit, New Mexico, *in* Pierce, F.W., Bolm, J.G., Eds., *Porphyry Copper Deposits of the American Cordillera*: Arizona Geological Society Digest 20, 464-472.
- Evans, A.M., 1993, Disseminated and stockwork deposits associated with plutonic intrusives *in* *Ore Geology and Industrial Minerals, An Introduction*, Third Edition: Blackwell Scientific Publications, 171-189.
- Gibson, M., Jolley, M., Barnicoat, A., Interpretation of the Western Ultra Deep Levels 3-D seismic survey: The Leading Edge, Society of Exploration Geophysicists, July 2000, 730-735.
- Hill, I.A., 1992, Better than Drilling? Some Shallow Seismic Reflection Case Histories: *Quarterly Journal of Engineering Geology*, **25**, 239-248.
- Juhlin, C., Palm, H., 1999, 3-d structure below Avro Island from high-resolution reflection seismic studies, southeastern Sweden: *Geophysics*, **64**, 662-667.

Kim, J.S. Moon, W.M., Lodha, G., Serzu, M., Soonawala, N., 1994, Imaging of Reflection Seismic Energy for Mapping Shallow Fracture Zones in Crystalline Rocks: *Geophysics*, **59**, 753-765.

Kolessar, J., 1982, The Tyrone Copper Deposit, Grant County New Mexico *in*. Titley, S.R., Eds., *Advances in the Geology of the Porphyry Copper Deposits, Southwestern North America: The University of Arizona Press*, 327-333.

Larner, K., Chambers, R., Yang, M., Lynn, W., Wai, W., 1983, Coherent noise in marine seismic data: *Geophysics*, **48**, 854-886.

Levin, S.A., 1989, Surface-consistent deconvolution: *Geophysics*, **54**, 1123-1133.

Milkereit, B., Eaton, D., Wu, J., Perron, G., Salisbury, M., Berrer, E.K., Morrison, G., 1996, Seismic Imaging of Massive Sulfide Deposits: Part II. Reflection Seismic Profiling: *Economic Geology and the Bulletin of the Society of Economic Geologists*, **91**, 829-834.

ProMAX 6.2 Reference Manual, Landmark Graphics Corporation, 1989-1996.

Salisbury, M., Milkereit, B., Bleeker, W., 1996, Seismic Imaging of Massive Sulfide Deposits: Part-I. Rock Properties: *Economic Geology and the Bulletin of the Society of Economic Geologists*, **91**, 821-828.

Stegen, R., personal communication, 15 June 1998.

Stuart, G., Jolley, S., Polome, L., Tucker, R., Application of 3-D seismic attributes analysis to mine planning: Target gold deposit, South Africa: *The Leading Edge, Society of Exploration Geophysicists*, July 2000, 736-742.

Telford, W.M., Geldart, L.P., Sheriff, R.E., 1990, *Applied Geophysics*, Second Edition: Cambridge University Press.

Yimaz, O., 1987, Seismic data processing, investigations in geophysics, volume 2: *Society of Exploration Geophysicists*.

Zelt, C.A., Smith, R.B., 1992, Seismic Traveltime Inversion for 2-D Crustal Velocity Structure: *Geophysical Journal International*, **108**, 16-34.